Open access • Proceedings Article • DOI:10.4271/2019-01-0085

Isobaric Combustion: A Potential Path to High Efficiency, in Combination with the Double Compression Expansion Engine (DCEE) Concept — Source link

Rafig Babayev, Moez Ben Houidi, Arne Andersson, Bengt Johansson

Institutions: King Abdullah University of Science and Technology, Volvo

Published on: 15 Jan 2019

Topics: Isobaric process

Isobaric Combustion: A Potential Path to High Efficiency, in Combination with the Double Compression Expansion Engine (DCEE) Concept

Thesis by

Rafig Babayev

In Partial Fulfillment of the Requirements

For the Degree of

Master of Science

King Abdullah University of Science and Technology

Thuwal, Kingdom of Saudi Arabia

November, 2018

EXAMINATION COMMITTEE PAGE

The thesis of Rafig Babayev is approved by the examination committee.

Committee Chairperson: Prof. Bengt Johansson

Committee Members: Prof. Aamir Farooq, Prof. Omar Knio

ABSTRACT

Isobaric Combustion: A Potential Path to High Efficiency, in Combination with the Double Compression Expansion Engine (DCEE) Concept

Rafig Babayev

The efficiency of an internal combustion engine is highly dependent on the peak pressure at which the engine operates. A new compound engine concept, the double compression expansion engine (DCEE), utilizes a two-stage compression and expansion cycle to reach ultrahigh efficiencies. This engine takes advantage of its high-integrity structure, which is adapted to high pressures, and the peak motored pressure reaches up to 300 bar. However, this makes the use of conventional combustion cycles, such as the Seiliger–Sabathe (mixed) or Otto (isochoric) cycles, not feasible as they involve a further pressure rise due to combustion. This study investigates the concept of isobaric combustion at relatively high peak pressures and compares this concept with traditional diesel combustion cycles in terms of efficiency and emissions. Multiple consecutive injections through a single injector are used for controlling the heat release rate profile to achieve isobaric heat addition. In this study, the intake pressure is varied to enable a comparison between the isobaric cases with different peak pressures, up to 150 bar, and the mixed cycle cases. Tests are performed at several different levels of EGR. The experiments are performed on a 12.8 L displacement 6-cylinder Volvo D13C500 engine utilizing a single

cylinder with a standard 17-compression-ratio piston. In this study, the cylinder represents the high-pressure unit of the DCEE. The fuel used in all the experiments is a standard EU diesel. In each target condition, the different injection strategies are compared with the total amount of fuel kept relatively constant. The results prove that the isobaric combustion concept is feasible with a traditional injection system and can achieve gross indicated efficiencies close to or higher than those of a conventional diesel combustion cycle. Moreover, the results show that with an isobaric cycle, heat transfer losses can be reduced by over 20%. However, the exhaust energy is higher, which can eventually be recovered in the second stage of expansion. Thus, this cycle could be suitable for the DCEE concept. The CO, UHC and soot emission levels are proven to be fairly similar to those of the conventional diesel combustion. However, the NOx emissions are significantly lower for the isobaric combustion.

TABLE OF CONTENTS

Page

LIST OF ABBREVIATIONS

ATDC	after top dead center
BDC	bottom dead center
BMEP	brake mean effective pressure
BP	back pressure
CAC	charge air cooler
CAD	crank angle degree
CDC	conventional diesel combustion
DCEE	double compression expansion engine
EGR	exhaust gas recirculation
EXMEP	exhaust mean effective pressure
FMEP	friction mean effective pressure
FuelMEP	fuel mean effective pressure
GHG	greenhouse gas
HD	heavy duty
HP	high pressure
HTMEP	heat transfer mean effective pressure
IMEPg	gross indicated mean effective pressure
IMEPn	net indicated mean effective pressure
Isobaric H	isobaric cycle at higher pressure
Isobaric L	isobaric cycle at lower pressure
LP	low pressure
NTP	normal temperature and pressure
PCP	peak cylinder pressure
PMEP	pumping mean effective pressure
PMP	peak motored pressure
SI	spark ignition
SOHC	single overhead cam
TDC	top dead center

LIST OF ILLUSTRATIONS

LIST OF TABLES

CHAPTER 1

INTRODUCTION

1.1 Motivation

The internal combustion engine efficiency is an important factor that significantly influenced the direction of engine research and has shaped engines to be as we know them today. However, recently, the research in this domain has started gaining momentum, owing to its direct impact on the greenhouse gas (GHG) emissions, from the transportation sector. The emissions of carbon dioxide (CO2), by far the most important GHG, are proportional to the fuel consumption of the vehicles, and thus, they are inversely proportional to the efficiency of the engines. The transportation sector accounts for over 14% of the world's GHG production [1]. In some countries, such as the US, it is the biggest contributor, being responsible for 28% of the total GHG emissions [2]. Heavy-duty (HD) diesel vehicles account for 25% of the transport CO2 emissions in the EU [3], and this number is only expected to increase, owing to the projected 45% increase in demand for HD vehicles by 2040 [4]. Furthermore, emissions are not the only driving force for the improvements in fuel efficiency. Road freight vehicles are commercial assets, the profitability of which directly depends on the fuel economy.

However, it is well documented in the literature that the fuel efficiency of HD vehicles has been stagnant for a number of years, owing to the fact that the main research interest has been in emissions reduction strategies, and not efficiency maximization, which is a

consequence of more strict emission regulations [5, 6, 7]. Nevertheless, several ways of increasing the fuel efficiency of engines have been proposed over the years. A large fraction of them focused on isochoric combustion, striving to approach the Otto cycle. However, none of them could achieve dramatic improvements in the brake thermal efficiency (BTE). The reason for this is that BTE depends on the losses in each cycle component, requiring a simultaneous optimization of the combustion, thermodynamic, gas exchange, and mechanical efficiencies. In other words, a theoretically ideal thermodynamic cycle does not necessarily translate into the most efficient real cycle. This study takes another approach at achieving high efficiencies, which is described in detail later in the text.

1.2 Split-Cycle Engine Concepts

A prospective solution to such a challenging task as finding a balance between individual efficiencies is a split-cycle engine concept. There have been several designs proposed. Among the more recent ones are the Scuderi split cycle (SSC) engine [8], the compact compression ignition (CCI) engine [9], “CryoPower” cryogenic split-cycle engine concept [10], and the double compression expansion engine (DCEE) concept [11].

All these designs differ from one another in a number of ways: The SSC engine has two similarly sized cylinders (compressor and expander), which have a small phase difference and are connected by a crossover port. The schematic of this engine is presented in Figure 1.1.

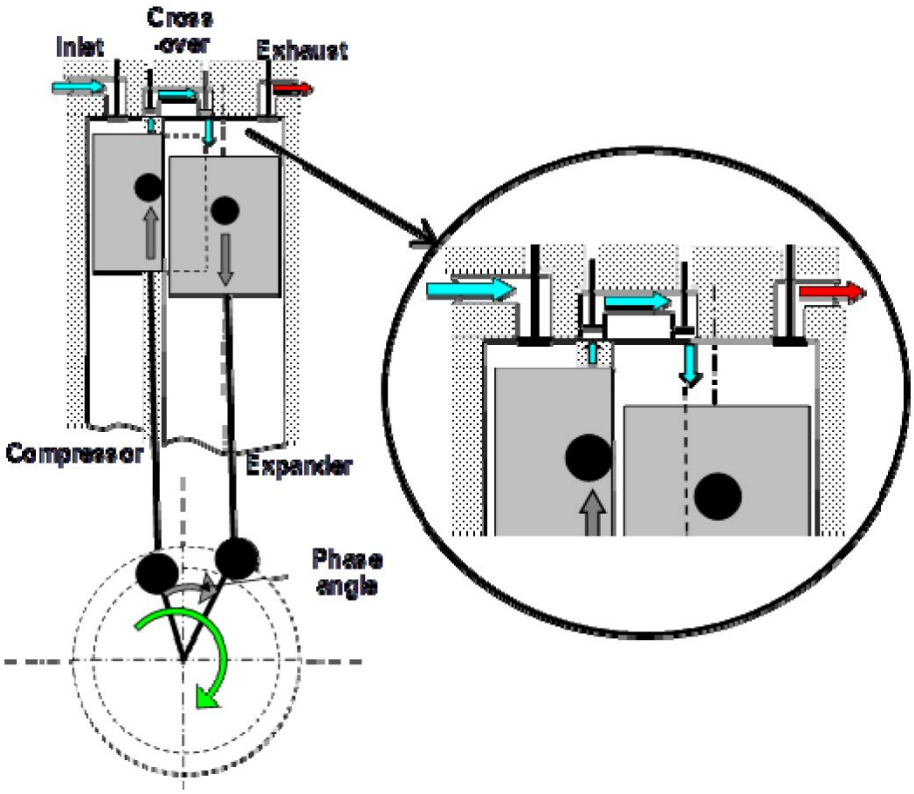

Figure 1.1. Schematic of the Scuderi split cycle (SSC) engine [8].

The CCI engine has three types of cylinders: intake, combustion, and exhaust cylinders. The operation, in a way, resembles a gas turbine, as the working fluid passes through each stage sequentially. The schematic of this engine is shown in Figure 1.2. In this figure, the blue components are one part, which reciprocates horizontally and represents the intake and exhaust pistons. The red parts are opposed pistons mounted on two counter-rotating crankshafts.

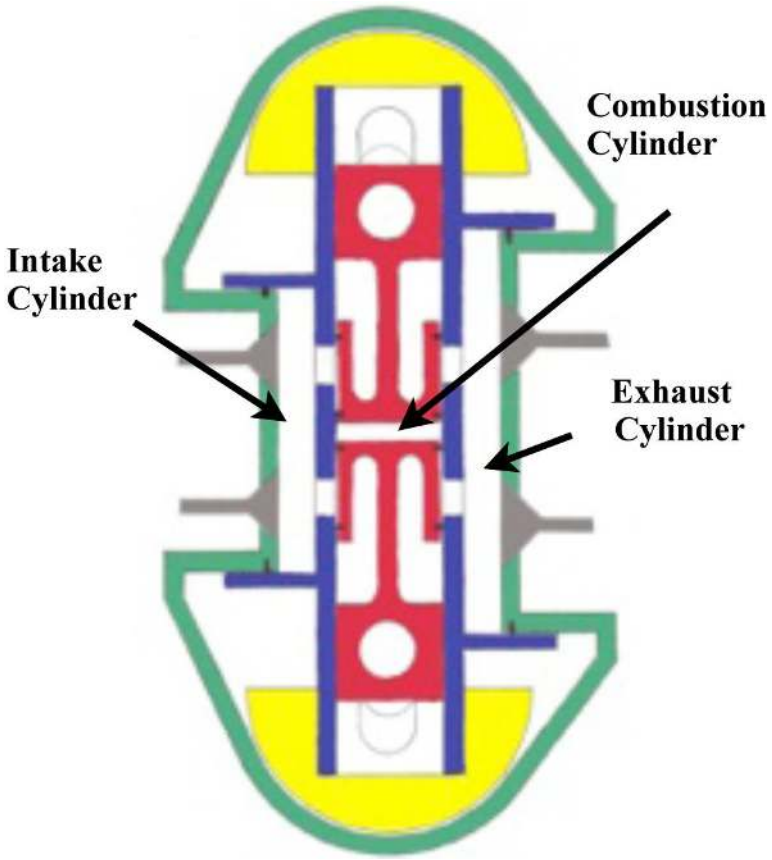

Figure 1.2. Schematic of the compact compressions ignition (CCI) engine [9].

The “CryoPower” concept utilizes an isothermal compressor and recuperator to achieve high thermal efficiency. The compression process can be carried out isothermally by injecting liquid nitrogen into the compressor cylinder. The schematic of a possible six-cylinder configuration of the “CryoPower” engine is presented in Figure 1.3. In this configuration, it has two compression and four power cylinder.

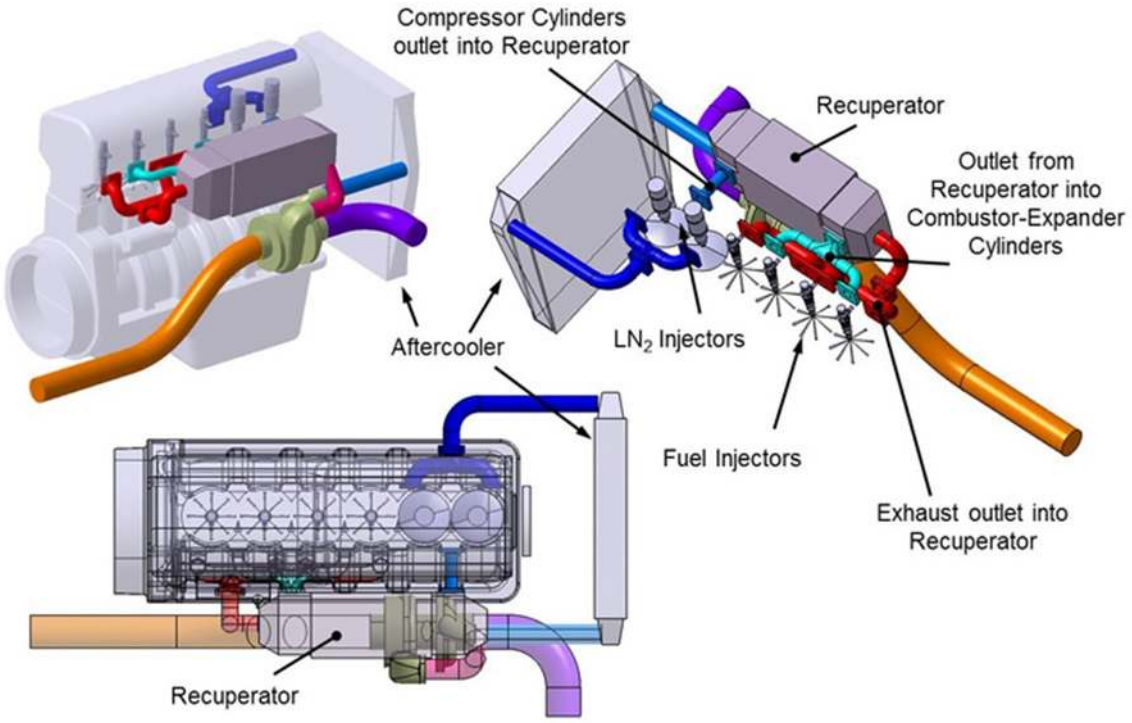

Figure 1.3. Schematic of the "CryoPower" cryogenic split-cycle engine concept [10].

1.3 Double Compression Expansion Engine (DCEE) Concept

1.3.1 The 4-4 Stroke Concept

The DCEE concept, introduced by Lam et al., differs from every other split-cycle engine in some aspect. Multiple numerical studies have been performed on the DCEE concept [11, 12, 13, 14], according to which, the concept is capable of achieving a brake efficiency of 56.0% at lambda 3.0. This novel engine concept consists of two cylinders, one operating at low pressures, and the other operating at high pressures. Both cylinders operate in 4-

stroke mode, hence the concept is called 4-4 stroke. Fuel injection and combustion occur in the high-pressure (HP) unit, which also accommodates the first stage of the expansion process, whereas the low-pressure (LP) unit is used as the second stage of the expansion. The size of the HP unit is limited as much as possible to reduce heat transfer and mechanical losses, whereas the LP unit is more similar to a conventional SI engine cylinder in terms of the associated low friction losses and larger displacement volume, because the temperatures during the second expansion stage are low. The LP unit also performs the first stage of the compression process, before transmitting the compressed air through a charge air cooler (CAC) into the HP unit, where the air is further compressed before combustion. The CAC is used to keep the temperatures at the BDC of the HP unit at sustainable levels, preventing excessive peak temperatures in the cycle. The exhaust gases of the HP unit are transmitted back to the LP unit through a crossover channel. The operation of the two cylinders is synchronized by setting a phase difference of 180˚. The DCEE concept is illustrated in Figure 1.4.

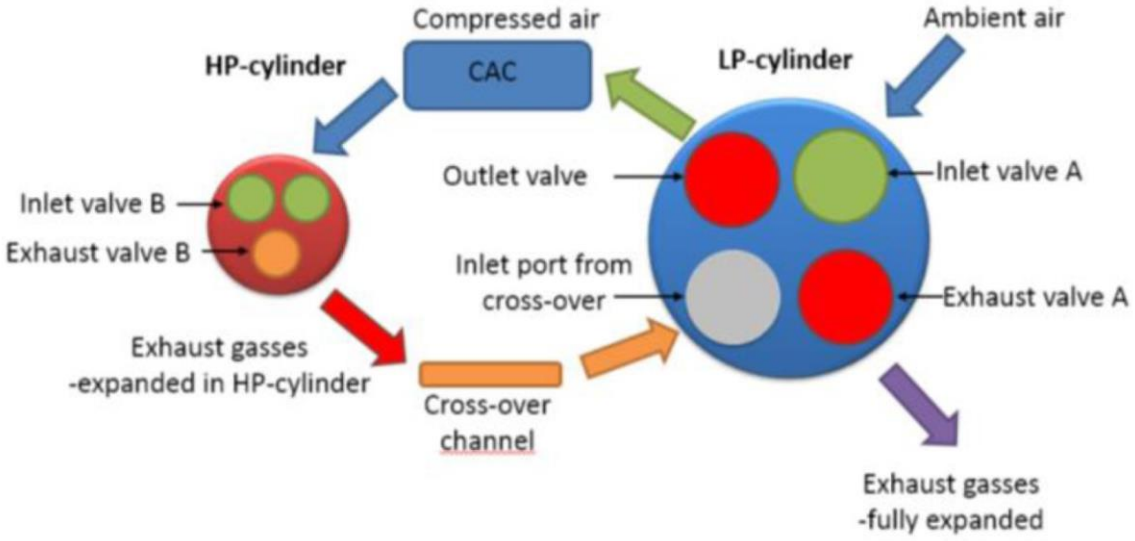

Figure 1.4. The 4-4 stroke DCEE concept system layout [11].

1.3.2 The 2-4-2 Stroke Concept

Another configuration of the DCEE is the 2-4-2 stroke concept. This variant of the engine has a similar operating principle to the 4-4 stroke concept, except, instead of using a single 4-stroke cylinder for both compression and expansion, this concept uses two separate 2-stroke cylinders: one for compression, and one for expansion. The advantages of the 2-4-2 stroke variant over the 4-4 stroke are: ability to achieve overexpansion without Miller-timing; more flexibility in mechanical balancing and use of exhaust gas aftertreatment systems. The illustration of the working principle of the 2-4-2 stroke DCEE concept is presented in Figure 1.5.

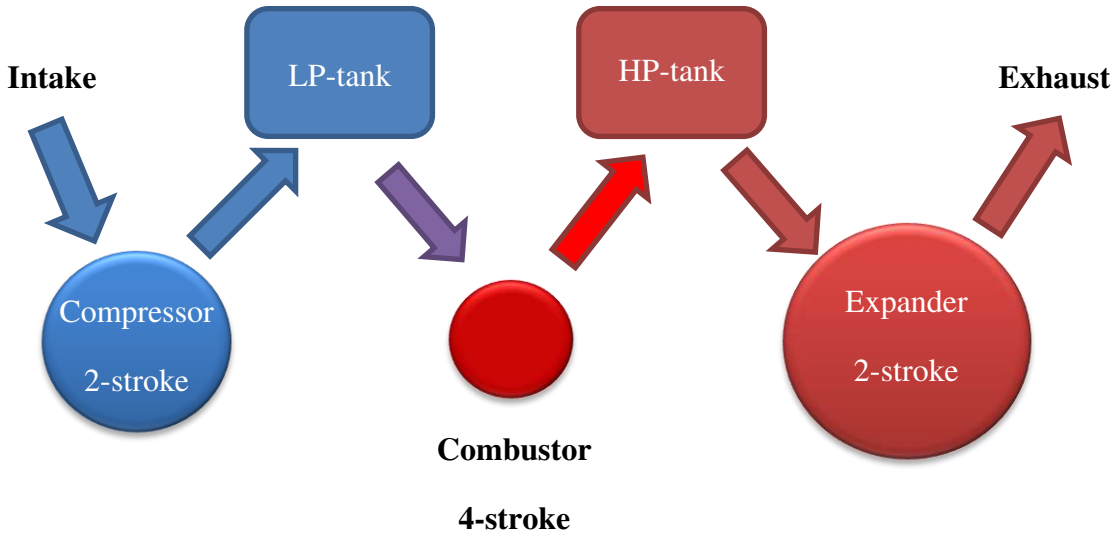

Figure 1.5. The 2-4-2 stroke DCEE concept system layout.

Figure 1.6 presents the P-V diagram of the ideal thermodynamic cycle that represents the operation of the three cylinders of the concept. The thermodynamic cycle is basically the ideal Brayton cycle, if the small volume shift of the combustor is disregarded. The compressor operates in a counter-clockwise loop, the combustor and expander operate in a clockwise loop. The gas exchange process is performed at constnat pressure. The ideal Brayton cycle that represents the DCEE concept operation is depicted in Figure 1.7.

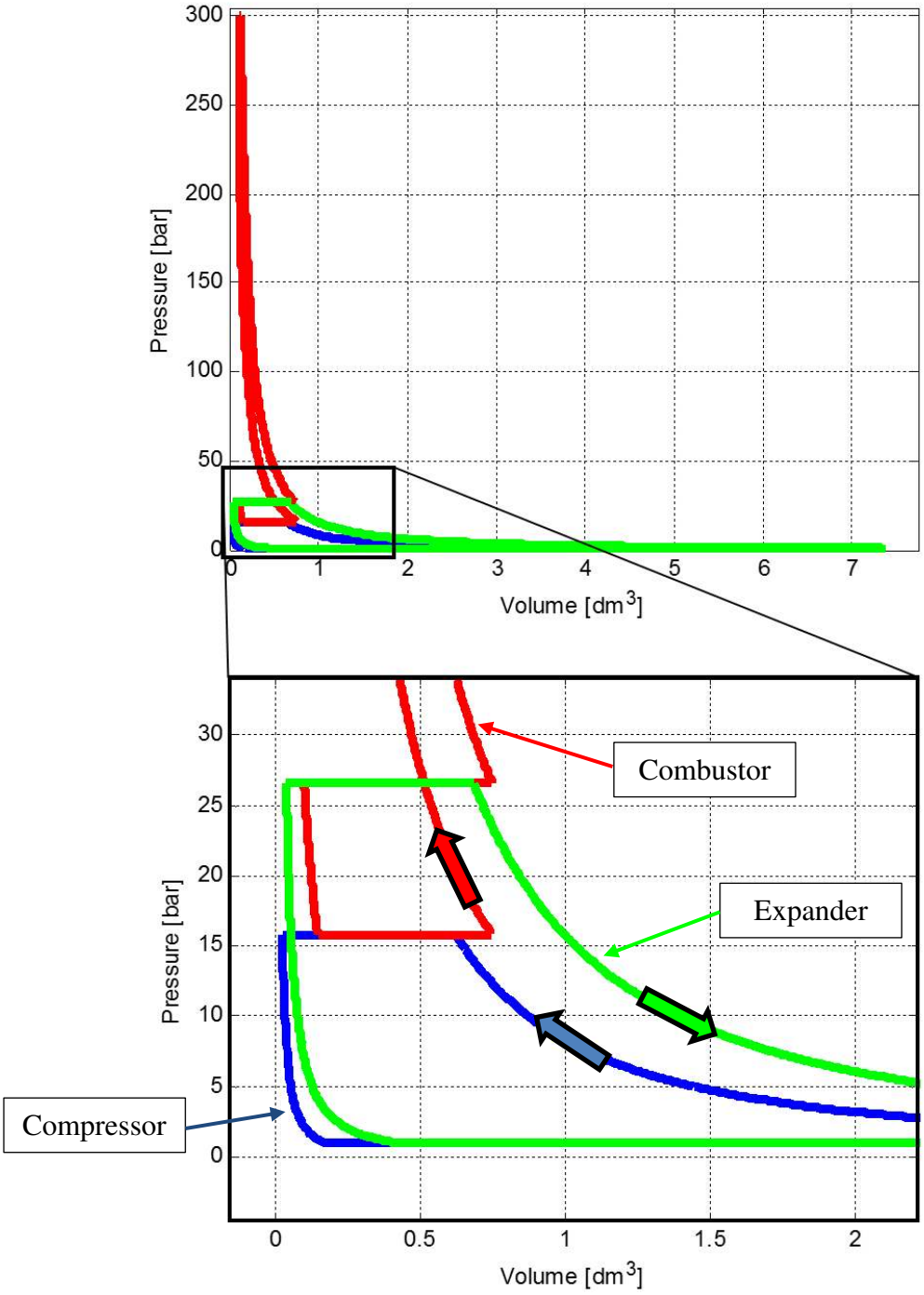

Figure 1.6. Idealized cycle of the 2-4-2 stroke DCEE concept.

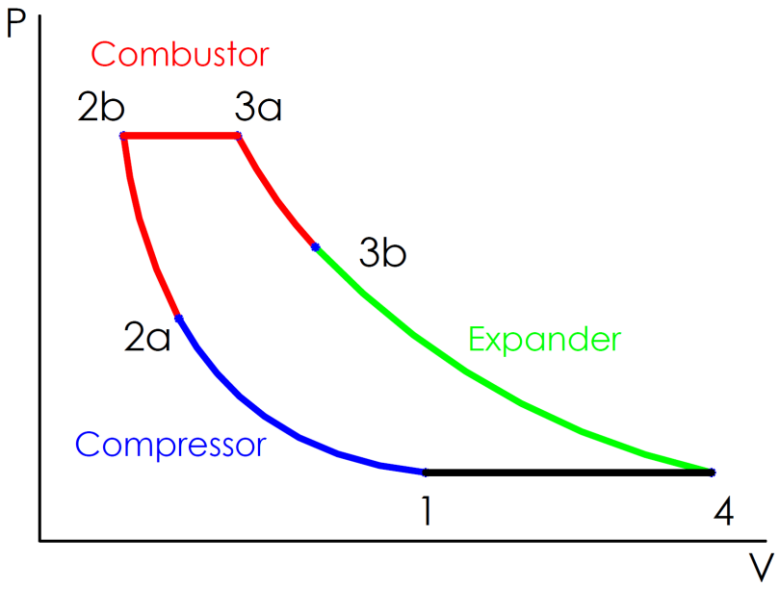

Figure 1.7. P-V diagram of the ideal Brayton cycle operated by the 2-4-2 stroke DCEE concept.

1.4 Isobaric Combustion

This study aims to determine the combustion cycle most suitable for the DCEE concept. Consequently, only the HP unit is considered as it is the only part of the engine that accommodates the combustion process. The DCEE relies on a high effective compression ratio to achieve higher efficiencies, and thus, it is expected to operate at remarkably high peak motored pressures (PMP) of 250–300 bar. However, this effectively means that there is no room for further pressure rise due to combustion. Most diesel engines rarely reach cylinder pressures larger than 200 bar. Operating at 250–300 bar requires certain modifications, whereas pressures higher than this are not yet achievable considering cost and friction loss standpoints. The solution is to implement a constant pressure cycle instead

of striving for constant volume cycles. It was shown by Okamoto and Uchida [15] that achieving cycles close to isobaric is possible using three injectors (Figure 1.8).

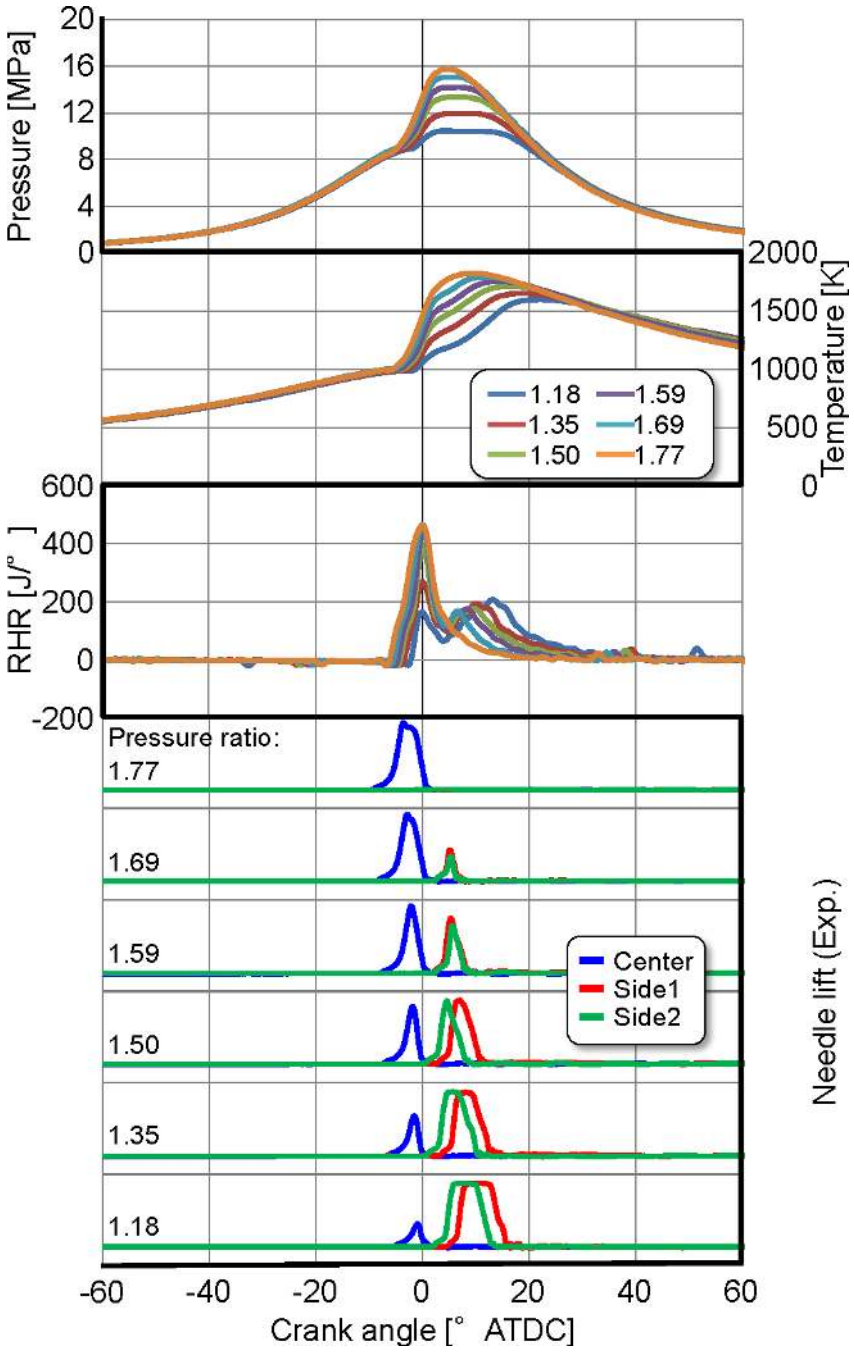

Figure 1.8. Different cycles realized by Okamoto and Uchida using a system of three injectors [15].

They were able to realize several different combustion cycles, which were classified according to different pressure ratios (r_p = peak cylinder pressure / compression pressure), starting from more isochoric combustion (r_p = 1.77) and reaching close to isobaric conditions (r_p = 1.18). In this study, the pressure ratio was further decreased to **1**, meaning heat addition was entirely isobaric. Furthermore, it is shown later that to achieve the heat release rate shapes necessary for the isobaric combustion cycle, three injectors are not necessary. A single conventional centrally mounted injector utilizing multiple consecutive injections can achieve similar shapes for the heat release rate as a system of multiple injectors can. The injection strategy used in a load sweep is illustrated in Figure 1.9, along with the resultant pressure and heat release rate traces. Even though, for a given compression ratio, the ideal thermodynamic efficiency of an isobaric cycle is lower than that of the isochoric or mixed cycles, it is shown by means of simple intuitive calculations, that under realistic boundary conditions, even idealized mixed and constant pressure cycles can have very similar results in terms of the thermodynamic efficiency. Furthermore, the detailed experimental results prove that at some conditions, the efficiency of the isobaric combustion cycle can exceed that of the mixed cycle because of second order effects, and simultaneously, an improvement in the emissions values can be achieved.

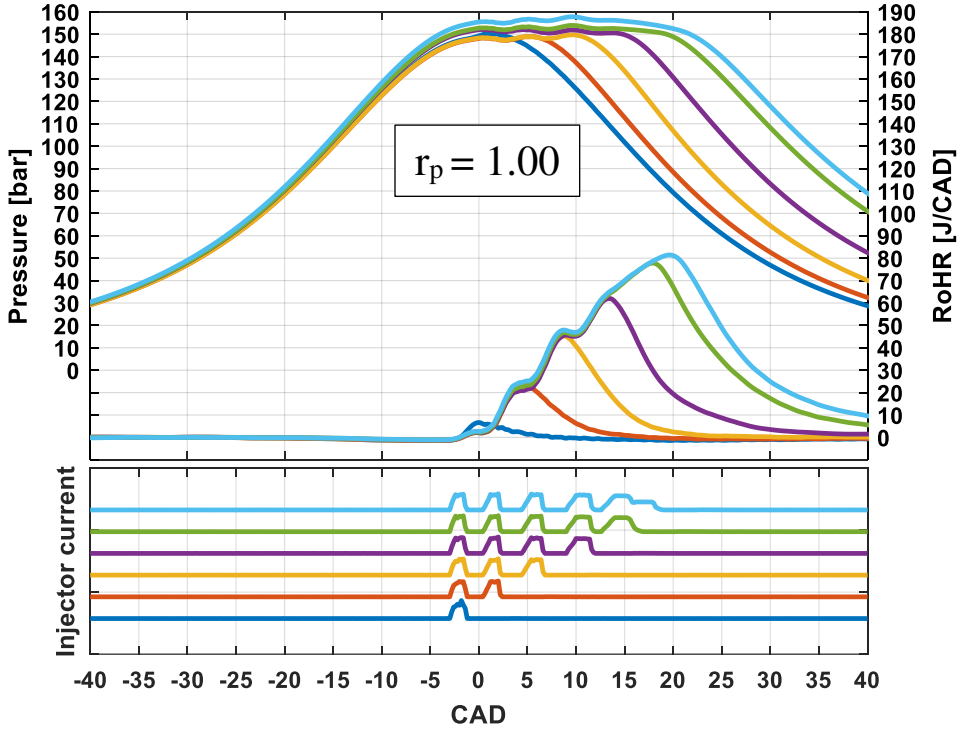

Figure 1.9. Injector current, pressure and rate of heat release traces for the load sweep with the isobaric combustion.

1.5 Objectives

The main objectives of this thesis are the following:

- Find out whether it is possible to achieve the isobaric combustion cycle using a conventional diesel fuel injection system, and what are limitations and challenges associated with this strategy.
- Identify whether the isobaric combustion cycle is more suitable for the DCEE concept than the conventional diesel combustion cycle.
- Compare the isobaric combustion cycle with the conventional diesel combustion cycle in terms of efficiency and emissions at different rates of EGR.

CHAPTER 2

CALCULATION OF EFFICIENCIES AND MEAN EFFECTIVE PRESSURES

2.1 Ideal Thermodynamic Cycles

Internal combustion engines are often studied on simple idealized models, which offer a clear distinction between the effects of different variables. There are two main ideal cycles that represent reciprocating engines: the ideal Otto cycle and the ideal Diesel cycle. Both these cycles are illustrated on a P–V diagram in Figure 2.1. The main difference between these cycles is that in the Otto cycle, heat addition is isochoric (constant volume), whereas in the Diesel cycle, the heat addition is isobaric (constant pressure).

Real diesel engines operating with conventional injection strategies can be approximated by the ideal mixed cycle (diagram B in Figure 2.1), which is a combination of the isochoric and isobaric cycles [16]. There are also other names for it, such as the dual cycle, Sabathe cycle, Seiliger cycle, or a combination of these.

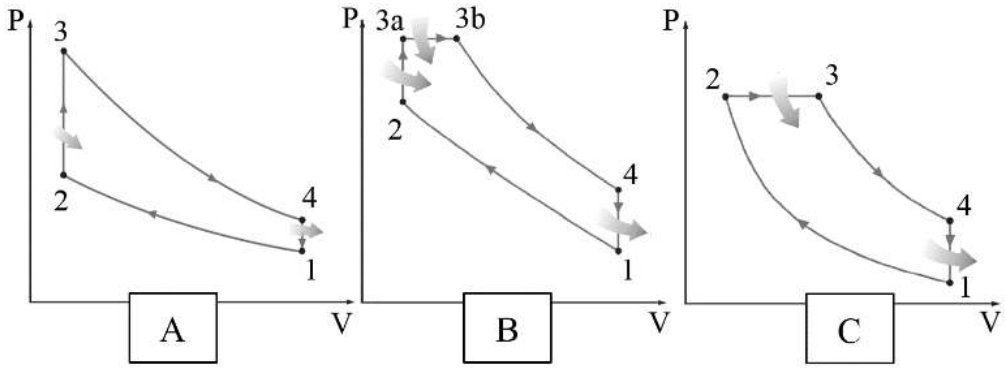

Figure 2.1. P–V diagram of an isochoric (A), mixed (B), and isobaric (C) cycle. Arrows indicate heat addition and heat rejection.

2.1.1 Ideal Mixed Cycle Efficiency

The ideal mixed cycle (Figure 2.1 B) can be broken down into five idealized processes:

1-2	Isentropic compression
2-3a	Constant-volume heat addition
3a-3b	Constant-pressure heat addition
3b-4	Isentropic expansion
4-1	Constant-volume heat rejection

Here, the fuel energy is transferred to the working fluid first isochorically, and then isobarically, which is a reasonable approximation to a conventional diesel combustion (CDC) cycle. This can be expressed by the following equation:

$$Q_{in} = m * c_v * (T_{3a} - T_2) + m * c_p * (T_{3b} - T_{3a}) \quad (1)$$

where m – Mass of the working fluid,

c_v – Specific heat at constant volume,

c_p – Specific heat at constant pressure.

The rejection of heat from the working fluid to the environment is performed in an isochoric manner, which can be expressed as follows:

$$Q_{out} = m * c_v * (T_4 - T_1) \tag{2}$$

Performing the energy balance on the system, the useful work on the piston can be calculated as follows:

$$W_{useful} = Q_{in} - Q_{out} \tag{3}$$

Then, the thermodynamic efficiency can be expressed as a ratio of the useful work and the total amount of energy transferred into the system:

$$\eta_{th} = \frac{W_{useful}}{Q_{in}} \tag{4}$$

In order to avoid the estimation of the temperatures at each point in the cycle, the following definitions are introduced:

$$r_p = \frac{P_{3a}}{P_2} \tag{5}$$

$$r_c = \frac{V_{3b}}{V_{3a}} \tag{6}$$

$$r = \frac{V_1}{V_2} \tag{7}$$

where P_2, P_{3a} – P pressures at the corresponding points in the cycle,

V_1, V_2, V_{3a}, V_{3b} – Volumes at the corresponding points in the cycle,

r_p – Pressure ratio during isochoric heat addition,

r_c – Cutoff ratio, which is the ratio of the volumes after and before the isobaric heat addition,

r – Compression ratio, which is the ratio of the combustion chamber volume at the start and the end of isentropic compression.

The temperatures at each point in the cycle can be expressed as follows:

$$T_2 = T_1 * r^{\gamma-1} \tag{8}$$

$$T_{3a} = T_1 * r^{\gamma-1} * r_p \tag{9}$$

$$T_{3b} = T_1 * r^{\gamma-1} * r_p * r_c \tag{10}$$

$$T_4 = T_1 * r_p * r_c^{\gamma} \tag{11}$$

where T_1, T_2, T_{3a}, T_{3b}, T_4 – Temperatures at the corresponding point in the cycle,

γ – Specific heat ratio of the working gas.

Consequently, the thermodynamic efficiency of this cycle can be expressed by the following equation [16]:

$$\eta_{th} = 1 - \frac{1}{r^{\gamma-1}} * \left(\frac{r_p * r_c^{\gamma} - 1}{r_p - 1 + \gamma * r_p * (r_c - 1)} \right) \quad (12)$$

2.1.2 Ideal Diesel (Isobaric) Cycle Efficiency

An isobaric cycle, which is the focus of the current thesis, can be represented by the ideal Diesel cycle shown in Figure 2.1 C.

It consists of the following four idealized processes:

1-2	Isentropic compression
2-3	Constant-pressure heat addition
3-4	Isentropic expansion
4-1	Constant-volume heat rejection

The heat addition process in this cycle occurs only at constant pressure conditions, which makes it a reasonable approximation for the real isobaric combustion cycle. The heat addition process in such a cycle can be expressed as:

$$Q_{in} = m * c_p * (T_3 - T_2) \quad (13)$$

All the steps in the calculation of the thermodynamic efficiency are similar to those for the ideal mixed cycle:

$$Q_{out} = m * c_v * (T_4 - T_1) \tag{14}$$

$$W_{useful} = Q_{in} - Q_{out} \tag{15}$$

$$\eta_{th} = \frac{W_{useful}}{Q_{in}} \tag{16}$$

$$r_c = \frac{V_3}{V_2} \tag{17}$$

$$T_2 = T_1 * r^{\gamma - 1} \tag{18}$$

$$T_3 = T_1 * r^{\gamma - 1} * r_c \tag{19}$$

$$T_4 = T_1 * r_c^{\gamma} \tag{20}$$

Finally, the thermodynamic efficiency of the ideal Diesel (isobaric) cycle is the following:

$$\eta_{th} = 1 - \frac{1}{r^{\gamma - 1}} * \left(\frac{r_c^{\gamma} - 1}{\gamma * (r_c - 1)} \right) \tag{21}$$

Equations 1 and 2 are derived from an ideal cycle analysis in which the working fluid is an ideal gas with constant heat capacity. These assumptions are needed to make a relatively simple comparison of the thermal efficiency of the different ideal cycles. As pointed out by Heywood et al., these equations should be used carefully as η_{th} is quite sensitive to the values of γ. In the following analysis, γ is estimated by calculating the slope of the logP–logV plot in the expansion stroke.

2.2 Real Cycle Mean Effective Pressures and Efficiency

This section discusses the efficiency calculations of real cycles. The following calculations correspond to the quantities presented in the results section. The exact method of the efficiency estimation is presented later in this section, after the definition of all the underlying quantities.

Potentially, the easiest way of understanding the energy flow in the engine is by referring to the Sankey diagram, as shown in Figure 2.2.

The energy flow was expressed in terms of the mean effective pressures (MEPs). The MEP is a quantity that represents a constant pressure that must act on the piston during the entire power stroke to generate the same amount of work as the actual pressure of the real cycle. All MEPs are expressed in units of pressure. In this study, the bar was chosen as a unit for the MEPs.

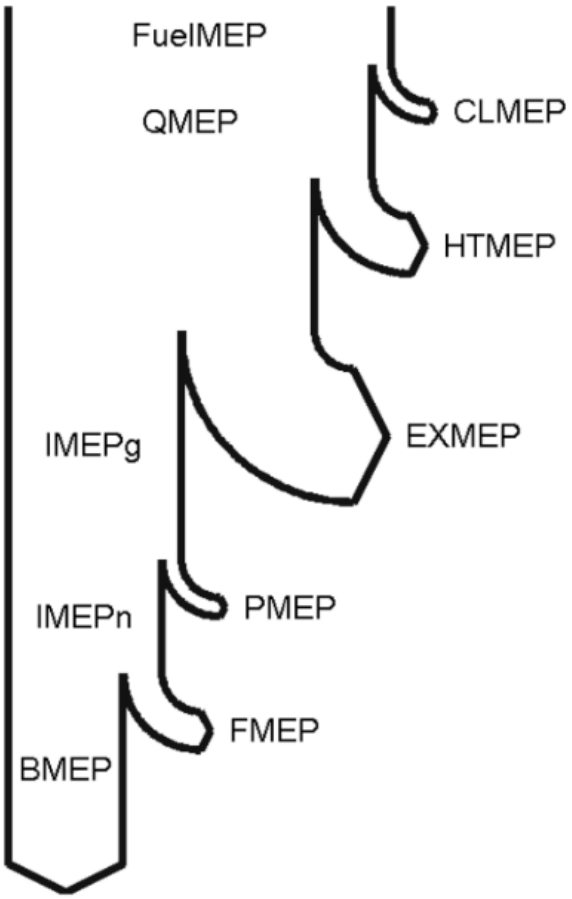

Figure 2.2. Energy flow in the engine, expressed as the mean effective pressures [17].

First, the fuel energy enters the system, and it is represented by FuelMEP as follows:

$$FuelMEP = \frac{m_f * Q_{LHV}}{V_D} \tag{22}$$

where m_f – Mass of fuel injected per cycle,

Q_{LHV} – Lower heating value of the fuel,

V_D – Displacement volume.

The mass of the fuel injected per cycle was calculated from the measured fuel, flow taking into account the engine speed and the fact that the engine is four-stroke.

The fuel chemical energy is transformed into thermal energy through the combustion process. This process is not perfect; some of the energy is lost owing to incomplete combustion, and it can be quantified as CLMEP. The resultant thermal energy entering the cycle is expressed by QMEP as follows:

$$QMEP = FuelMEP * \eta_c \tag{23}$$

$$CLMEP = FuelMEP - QMEP \tag{24}$$

where η_c – Combustion efficiency.

The combustion efficiency was calculated from the emissions data, based on the following equation [17]:

$$\eta_c = 1 - \left[\frac{1 + \lambda * AF_s}{Q_{LHV} * M_p} * \sum \left(M_i * x_i * Q_{LHV\,i}\right)\right] \tag{25}$$

where λ – Air–fuel equivalence ratio,

AF_s – Stoichiometric air–fuel ratio,

M_p – Total molar mass of the exhaust gas,

M_i – Molar mass of each component in the exhaust gas,

x_i – Wet molar concentration of each component in the exhaust gas,

$Q_{LHV\,i}$ – Lower heating value of each component in the exhaust gas.

The air–fuel equivalence ratio λ was calculated from the emissions according to [17]:

$$\lambda = \frac{1}{2\left(a+\frac{b}{4}-\frac{c}{2}\right)} * \left\{ \begin{matrix} \frac{a}{a\,x_{CaHbOc}+(1-x_{H2O})(x^*_{CO}+x^*_{CO2})} \\ *\,[c\,x_{CaHbOc}+x_{H2O}+(1-x_{H2O})(2x^*_{CO2}+x^*_{CO}+2x^*_{O2}+x^*_{NO}+2x^*_{NO2})]-c \end{matrix} \right\} \quad (26)$$

where x_i^* - Dry concentration of each component in the exhaust gas.

Subsequently, we consider the heat transfer mean effective pressure, which represents the total amount of heat lost to the walls of the combustion chamber via convection and radiation. The HTMEP in this study was estimated from the energy balance of the system. For the sake of clarity, the EXMEP and IMEPg are defined first, followed by the HTMEP.

The EXMEP represents the heat lost to the exhaust owing to incomplete extraction of the thermal energy of the working fluid by the piston. It is expressed by the following formula:

$$EXMEP = \frac{H_{exh}}{V_D} \quad (27)$$

where H_{exh} is the enthalpy of the exhaust gases, which was calculated using the following equation [18]:

$$H_{exh} = m_{exh} * (c_{p_{exh.gas\ @\ T_{exh}}} * T_{exh} - c_{p_{int.gas\ @\ T_{BDC}}} * T_{BDC}) \quad (28)$$

where m_{exh} – Mass per cycle of the gases in the exhaust,

$c_{p_{exh.gas\ @\ T_{exh}}}$ – Specific heat at constant pressure of exhaust gas estimated for the temperature measured in the exhaust,

T_{exh} – Temperature of the exhaust gases,

$c_{p_{int.gas\ @\ T_{BDC}}}$ – Specific heat at constant pressure of the intake gas estimated for the temperature at the bottom dead center,

T_{BDC} – Temperature of the gases at the bottom dead center.

Here, the temperature at the bottom dead center was assumed to be the same as the temperature measured in the intake pipe. The mass of the exhaust gases per cycle, m_{exh}, was calculated for the exhaust pipe located immediately after the exhaust manifold by summing up the mass of fuel injected and mass of air admitted into the cylinder per cycle. This way, the energy balance could be performed for the engine only, eliminating the unwanted effects of other test cell components such as the EGR cooler and losses in the piping.

The last important quantity in the context of the DCEE concept is the gross indicated mean effective pressure, IMEPg. It represents the work extracted by the piston from the working fluid in each cycle. IMEPg was calculated by integrating the pressure trace over the compression and expansion stroke as follows:

$$IMEP_g = \frac{W_{Comp} + W_{Exp}}{V_D} = \frac{1}{V_D} * \int_{180}^{540} PdV \quad (29)$$

The net indicated mean effective pressure, IMEPn, represents the useful work on the piston; however, in contrast to IMEPg, it also takes into account the inlet and exhaust strokes as follows:

$$IMEP_n = \frac{W_{Comp} + W_{Exp} + W_{Exh} + W_{Inl}}{V_D} = \frac{1}{V_D} * \int_{0}^{720} PdV \quad (30)$$

This parameter was also calculated, even though it plays a less significant role in the context of DCEE, because the gas exchange loop is significantly different in the presence of the second stage of expansion.

$$PMEP = IMEP_n - IMEP_g \quad (31)$$

where PMEP – Pumping mean effective pressure.

At this point, all the energy losses in the process of converting the chemical energy of the fuel into the gross indicated work on the piston are known, except for the heat transfer losses to the walls, which can be estimated by performing the energy balance as follows:

$$HTMEP = FuelMEP - CLMEP - EXMEP - IMEP_g \quad (32)$$

Finally, the gross indicated efficiency used in this work when comparing the efficiencies of different cycles was estimated based on the following equation:

$$\eta_{GI} = \frac{IMEPg}{FuelMEP} \tag{33}$$

This definition was chosen as it gives the most suitable estimation of the efficiency of the high-pressure unit of the DCEE concept.

The friction losses were estimated using the following relation:

$$FMEP = BMEP - IMEP_n \tag{34}$$

where FMEP – Friction mean effective pressure,

BMEP – Brake mean effective pressure calculated from the brake power generated by the engine.

CHAPTER 3

HEAT RELEASE ANALYSIS

The apparent heat released during combustion process is calculated using the following equation:

$$\frac{dQ_{HR}}{d\theta} = \frac{\gamma}{\gamma - 1} P \frac{dV}{d\theta} + \frac{1}{\gamma - 1} V \frac{dP}{d\theta} + \frac{dQ_{HT}}{d\theta} + \frac{dQ_{Cr}}{d\theta} + \frac{dQ_{Bl}}{d\theta} \qquad (35)$$

where γ – specific heat ratio,

P – in-cylinder pressure,

V – cylinder volume,

θ – crank angle degree,

Q_{HT} – heat transfer losses,

Q_{Cr} – crevice losses,

Q_{Bl} – blow-by losses.

3.1 Cylinder Volume Variation Modeling

As seen from the Equation 35, in order to calculate the heat release rate, first, it is necessary to model the cylinder volume as a function of crank angle. Figure 3.1 presents the illustration of the crank slider mechanism

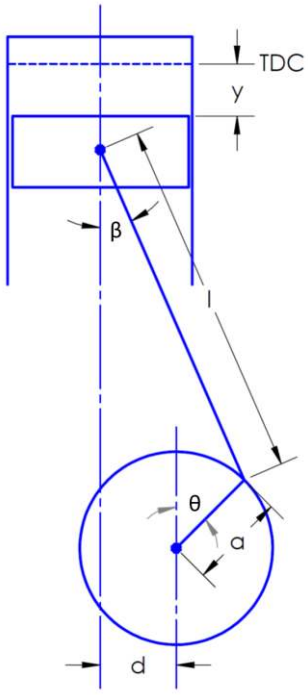

Figure 3.1. Crank slider geometry.

The piston location *y* can be expressed as

$$y = l + a - (l\cos\beta + a\cos\theta) \tag{36}$$

which can be rewritten as

$$y = a\left(1 - \cos\theta + \frac{l}{a}(1 - \cos\beta)\right) \quad (37)$$

Taking into account the crank offset and trigonometric identities as follows

$$\sin\beta = \frac{a}{l}\sin\theta - \frac{d}{l} \quad (38)$$

$$\sin^2\beta + \cos^2\beta = 1 \quad (39)$$

the following equation can be derived

$$y = a\left(1 - \cos\theta + \frac{l}{a} - \frac{l}{a}\sqrt{1 - \left(\frac{a}{l}\sin\theta - \frac{d}{l}\right)^2}\right) \quad (40)$$

Thus, the cylinder volume as a function of *y* can be expressed as

$$V = V_C + \frac{V_D}{2}\left(1 - \cos\theta + \frac{l}{a} - \frac{l}{a}\sqrt{1 - \left(\frac{a}{l}\sin\theta - \frac{d}{l}\right)^2}\right) \quad (41)$$

where V_C – Compression volume,

V_D – Displacement volume.

Differentiating the Equation 41 with respect to θ yields

$$\frac{dV}{d\theta} = \frac{V_D}{2}\sin\theta\left(1 + \frac{\cos\theta}{\sqrt{\frac{l^2}{a^2} - \sin^2\theta}}\right) \tag{42}$$

It should be noted that this equation does not take into account the crank offset, however, the error introduced by this approximation is negligibly small.

3.2 Pressure Signal Adjustments

3.2.1 Pegging

In-cylinder pressure is measured using a water-cooled KISTLER Type 7061C pressure sensor. It is, essentially, a piezoelectric transducer, and hence, the output signal is referenced to an arbitrary ground. As a result, the pressure signal is "floating" and needs to be referenced to a known value at some point in an engine cycle. This process is called pegging. There is a multitude of pegging methods. In this study, the pressure at the inlet bottom dead center is set to an absolute pressure measured in the intake pipe. This is a reasonable approximation, because the engine speed is relatively low (1200 RPM) and the inlet system is untuned, meaning, the pressure waves are not taken advantage of, and the in-cylinder pressure at the inlet valve closing is similar to the pressure in the intake pipe.

3.2.2 Phase Offset

The crank encoder used is Leine & Linde RSI 503 incremental shaft encoder. It gives a high resolution data on the engine crank position. The working principle of the encoder is based on photoelectric scanning of a graduated code disk. The grating on the disk is made using photolithographic processes enabling very high levels of precision. However, the absolute crank position must be calibrated. In this study, it is done like so: a number of motored cycles is recorded and averaged; then, the RoHR trace is obtained by performing a full heat release analysis; after that, the phase offset is varied until the RoHR trace is a horizontal line and close to zero. By doing so, the TDC offset was found to be -0.4 CAD.

3.3 Heat Transfer Losses

The heat transfer losses were estimated using the Woschni correlation [19]. The convective heat transfer coefficient according to Woschni is:

$$h_c \left[\frac{W}{m^2 \times K}\right] = 3.26\, B\,[m]^{-0.2} \times P[kPa]^{0.8} \times T[K]^{-0.55} \times w\left[\frac{m}{s}\right]^{0.8} \qquad (43)$$

where B – Cylinder bore,

P – Instantaneous in-cylinder pressure,

T – Instantaneous in-cylinder temperature,

w – Average cylinder gas velocity.

The average cylinder gas velocity *w* from Equation 43 is determined for a four-stroke, water-cooled, four-valve direct-injection CI engine without swirl according to:

$$w = C_1\overline{S_p} + C_2\frac{V_d\,T_r}{P_r\,V_r}(P - P_m) \tag{44}$$

where $\overline{S_p}$ – Average piston speed,

V_d – Displaced volume,

P – Instantaneous in-cylinder pressure,

P_r – The working fluid pressure at inlet valve closing,

T_r – The working fluid temperature at inlet valve closing,

V_r – The working fluid volume at inlet valve closing,

P_m – The motored pressure at the same CAD as P.

The coefficients C_1 and C_2 are determined according to:

Gas exchange period	$C_1 = 6.18$	$C_2 = 0$
Compression period	$C_1 = 2.28$	$C_2 = 0$

Combustion and expansion period	$C_1 = 2.28$	$C_2 = 3.24 * 10^{-3}$

Then, the heat transfer can be calculated using the Newton's law of cooling according to:

$$Q_{HT} = h_c\,(T - T_{wall}) \tag{45}$$

where T_{wall} – The temperature of the walls of the cylinder, assumed to be equal to the temperature of the cooling water in the current study.

The crevice and blowby effects are minimal in the current test cell. However, they were estimated according to Heywood et al. [20]

CHAPTER 4

EXPERIMENTAL SETUP AND TEST CONDITIONS

4.1 Experimental Setup

The experiments were performed on the KAUST-Volvo single cylinder research engine. A Volvo D13C500 6-cylinder engine was modified by deactivating the valves of five out of six cylinders and disconnecting the cylinders from the intake and exhaust systems. The engine was installed on a test cell designed by MESA Engine Solutions [21]. The image of the test cell is shown in Figure 4.1. The schematic of the experimental setup is shown in Figure 4.2.

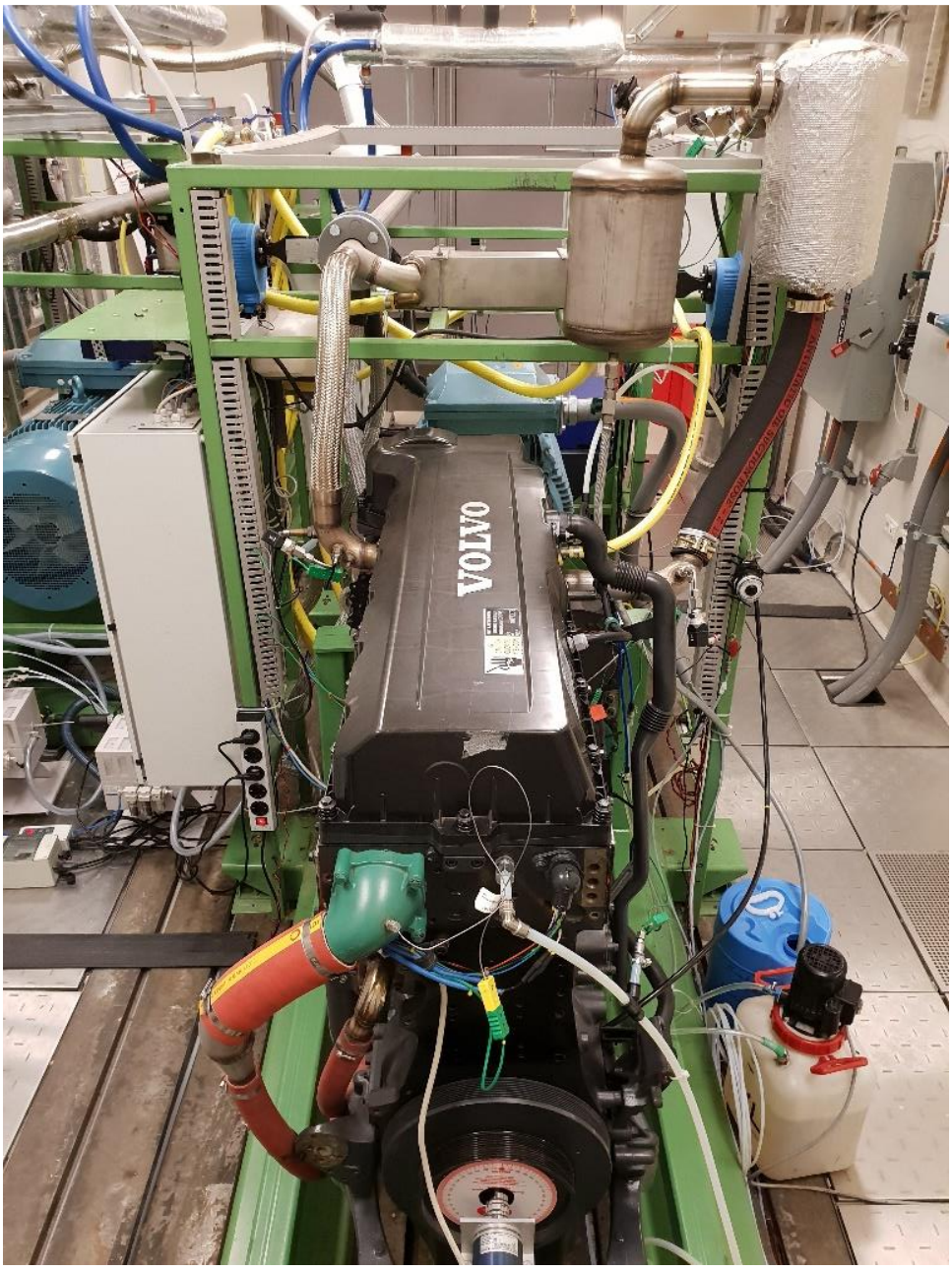

Figure 4.1. Image of the research test cell.

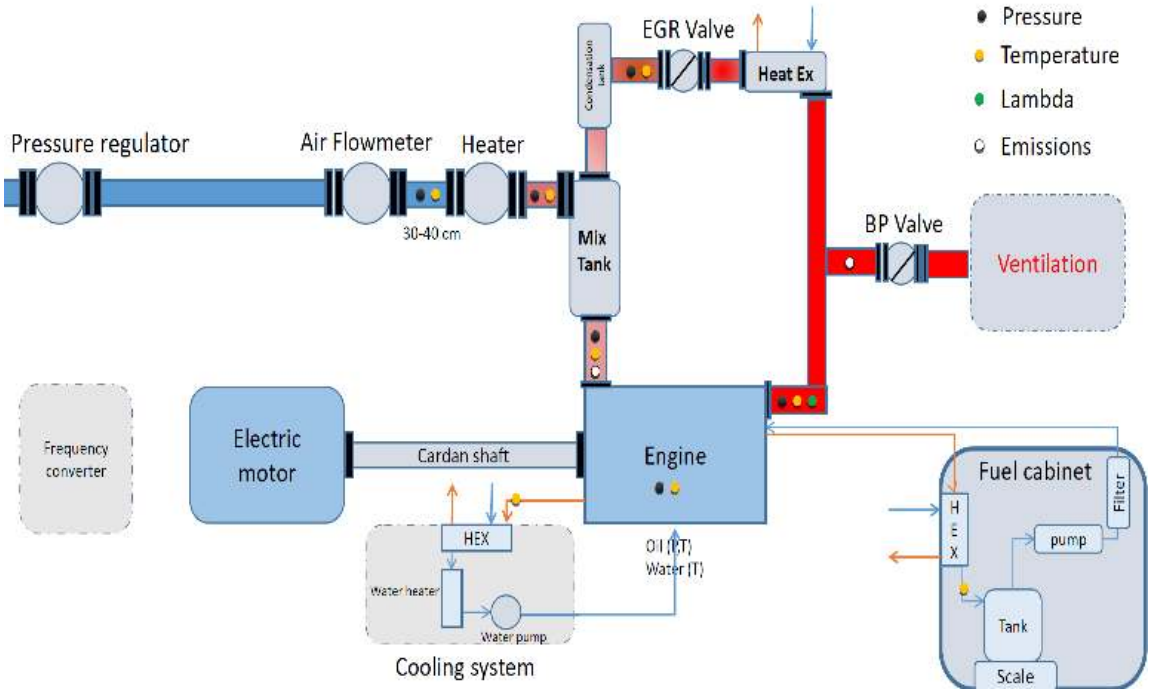

Figure 4.2. Schematic of the research test cell.

Base Engine Configuration	Single cylinder / 4 stroke
Displacement Volume	2.13 L
Stroke	158 mm
Bore	131 mm
Connecting Rod	255 mm
Compression ratio	17:1
Cam / Valve Configuration	SOHC / 4 valves per cylinder
Fuel Injection System	Common rail (2700 bar max P)

Table 4.1. Engine specifications.

The carbon monoxide (CO), unburned hydrocarbons (UHC), and nitrogen oxides (NOx) emissions were measured using the HORIBA MEXA-ONE-RS Motor Exhaust Gas

Analyzer. The range of each measurement component depends on the span gases concentration, which are reported below:

- CO – 4960 ppm
- CO2 – 18.45 vol%
- O2 – 20.00 vol%
- CH4 – 977 ppm
- NO – 8200 ppm

The soot emissions were measured using the AVL Micro Soot Sensor. The test cell was connected to a high-pressure air compressor, and a pressure regulator is used on the intake line to control the flow feeding the engine. The intake, EGR, and back pressure valves were controlled independently. The back pressure in all the experiments was set to a value higher than the intake pressure. This allowed the recirculation of the exhaust gases and simulation of the pressure drop typical of that in a turbocharger. This led to slightly conservative but reliable efficiency values.

4.2 Test Conditions

4.2.1 First Set of Experiments (Low Load)

The experimental strategy implemented in this study was chosen to enable comparison between the CDC and isobaric cycles in scenarios where the peak cylinder pressure of the HP unit of the DCEE concept is restricted. This was done to simulate conditions that the DCEE concept strives to achieve, namely, maximizing the efficiency by utilizing a very high effective compression ratio, and simultaneously minimizing the losses associated with high peak cylinder pressures (friction, heat transfer), while maintaining a reasonable level of emissions. In addition, in this manner, the effect of the peak cylinder pressure on the efficiency and emissions can also be observed.

The first set of experiments consists of three combustion cycles: a conventional diesel combustion (CDC) cycle and two isobaric combustion cycles (Isobaric L and Isobaric H).

At an intake pressure equal to 1 bar-absolute, two cases were studied:

- CDC – Conventional diesel combustion cycle in which the heat addition is first near-isochoric and then near-isobaric with the peak motored pressure close to 50 bar and the peak cylinder pressure (PCP) after combustion reaching 68 bar.
- Isobaric L – Isobaric heat addition with the PCP limited at 50 bar.

At the intake pressure equal to 1.45 bar-absolute, one more isobaric case was studied:

- Isobaric H – Isobaric heat addition at the same pressure level that the CDC reaches after combustion, i.e., 68 bar.

Each operating point was studied at three different levels of EGR—0%, 17%, and 39%—to investigate its effect on the system efficiency and emissions. This resulted in a total of nine cases. The amount of fuel injected per cycle in all the cases was kept close to constant at 50–55 [mg/cycle] to enable direct comparison of the energy flow in the system, as well as the efficiencies. The air–fuel equivalence ratio in the CDC and Isobaric L cases was equal to 3. The Isobaric H case however, had a lambda of 4.1, because the intake pressure was increased, leading to a larger amount of air entering the engine and a fixed amount of fuel added per cycle. The equivalence ratios of all operating points are summarized in Appendix B. The injection pressure was kept constant in all nine cases, equal to 1500 bar.

The CDC cycles were achieved with two injections. The first pilot injection was used to reduce the pressure rise rate during the combustion. First, it helped suppress the pressure oscillations that resulted in a knock-like behavior and an increased noise level. Second, it helped in obtaining more consistent rates of heat release.

Four injections, separated by short pauses, were required to achieve isobaric heat addition at moderate-to-high loads. The heat release rate shape was controlled by manually adjusting the injection timings and durations until the desired shape was achieved. The details of the injection strategies implemented can be seen in Figures 7.1, 7.2, and 7.3. As the percentage of EGR was increased, the injection timings had to be adjusted to achieve similar pressure traces with different EGR levels. In general, more exhaust fed back to the

intake decreased the reactivity of the charge, requiring a slight advancement in the injection timings. This was especially noticeable at 39%-EGR. The MEPs are listed in Appendix A.

4.2.2 Second Set of Experiments (High Load)

The second set of experiments was performed in a similar manner as the first one but at much higher pressures. The injection pressure remained the same, i.e., 1500 bar. The intake pressure was raised to 2.4 bar-absolute for the CDC and Isobaric L cases. For the Isobaric H case, the pressure was slightly more than 3.1 bar. The peak motored pressure reached 120 bar for the CDC and Isobaric L cycles, and 150 bar for the Isobaric H cycles. For the best efficiency, it was decided to keep the lambda close to 3. It has been shown before that high dilution enables high thermodynamic efficiencies owing to the minimizing of the heat transfer losses [22]. Because the amount of air was significantly higher than in the first set of experiments, the mass of fuel injected per cycle was increased as well, up to 110 mg/cycle on average, which enabled much higher IMEPs. The MEPs are listed in Appendix A.

In second set of experiments, three different rates of EGR were also studied: 0%, 10% and 52%. A higher EGR limit was chosen such that lambda is always constrained to values above 1.8, thereby avoiding excessive soot formation.

In the CDC cases, a three-injection strategy was utilized. The pilot injection was used for the same reason as in the first set of experiments. The third injection was utilized for two

reasons. First, the post injection promoted a pressure rise of up to 150 bar in a more isochoric manner, as the further increase in the duration of the second injection lead to higher cutoff ratios, thereby making the CDC lean toward a more isobaric cycle. Second, post injections have been known for decreasing soot emissions and are a common practice currently [23]. The equivalence ratio for all nine cases are reported in Appendix B.

The engine speed and intake temperature in all experiments were set to 1200 RPM and 18°C, respectively.

CHAPTER 5

IDEALIZED CYCLE EFFICIENCY AND RELEVANT RATIOS

This section describes the evaluation of the efficiency of the CDC, Isobaric L, and Isobaric H cycles under ideal conditions. An "envelope" cycle was fit onto the real in-cylinder pressure data. In this manner, the maximum theoretical efficiency of each cycle could be evaluated, and the effects of different parameters could be observed more clearly. In addition, the pressure and temperature at the end of the expansion stroke were also taken into account as these quantities represent the amount of energy that will be available for the LP unit of the DCEE. The higher these values are, the more additional work will be possible to be extracted in the second step of the expansion process.

5.1 Conventional Diesel Combustion Cycle

First, the conventional mixed cycle with the PCP of 150 bar and no EGR was represented with an idealized cycle, as discussed previously. The Log P–V diagram of this case is shown in Figure 5.1.

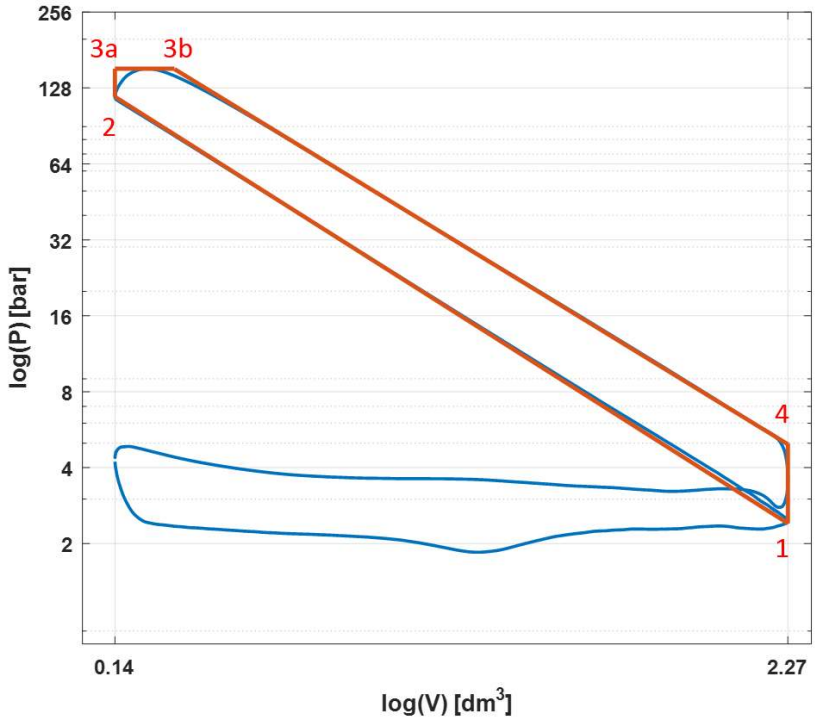

Figure 5.1. Log P–V diagram of the CDC cycle at 2.4 bar intake pressure and 0% EGR, and the corresponding idealized mixed cycle.

The ideal thermodynamic efficiency of the mixed combustion cycle was estimated using Equation 12, and its value was 60.4%. The pressure and temperature at point 4 are 4.9 bar and 422 K, respectively. The theoretical temperature at the end of the expansion was calculated from the pressure trace using the ideal gas law.

5.2 Isobaric L Cycle

Subsequently, we consider the isobaric combustion case at the pressure equal to the PMP of the CDC case (Isobaric L). It is depicted in Figure 5.2.

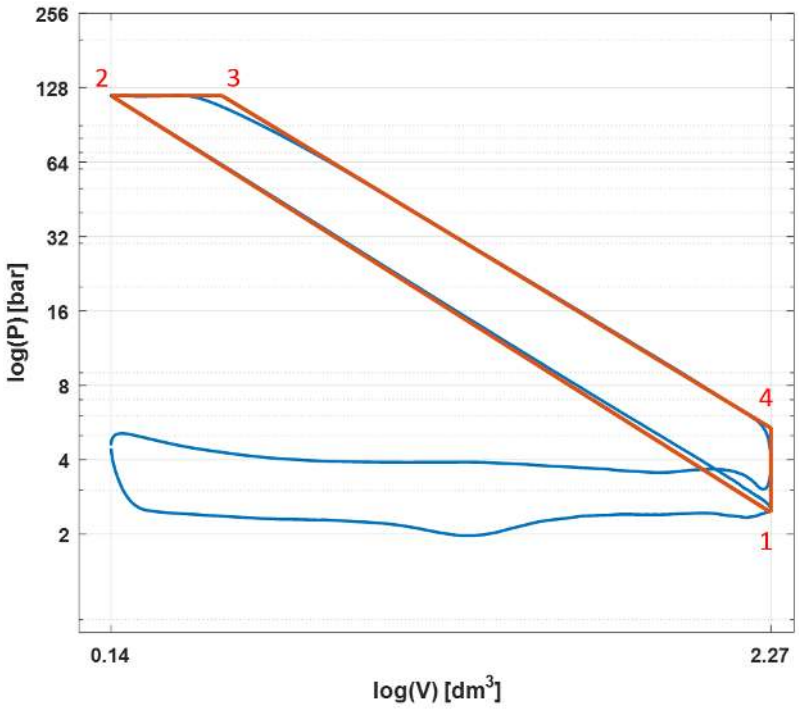

Figure 5.2. Log P–V diagram of the real isobaric combustion cycle at 2.4 bar intake pressure and 0% EGR, and the corresponding ideal diesel cycle.

The ideal thermodynamic efficiency of this cycle was estimated in accordance with the previous discussions using Equation 21, yielding a value of 56.6%. This value is significantly lower than that of the mixed cycle, already suggesting that the cycle efficiency of its real counterpart is also expected to be significantly lower. The pressure and temperature at point 5 were estimated to be 5.4 bar and 432 K, respectively.

5.3 Isobaric H Cycle

Finally, the exact same analysis was performed for the isobaric case with the constant pressure heat addition taking place at the pressures equal to those in the PCP of the CDC case (Isobaric H). This cycle, along with its ideal counterpart, is depicted in Figure 5.3.

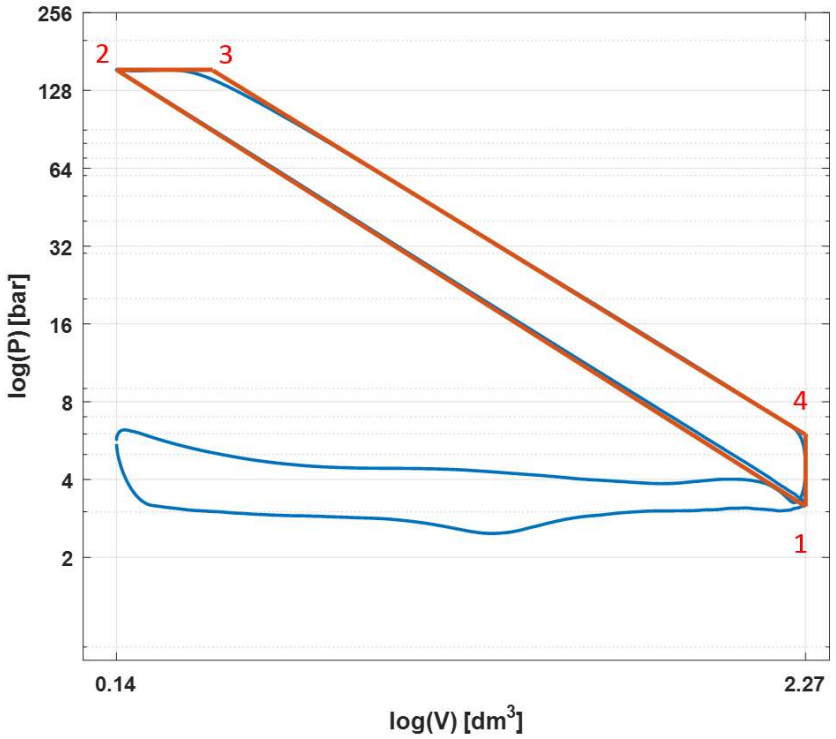

Figure 5.3. Log P–V diagram of the real isobaric combustion cycle at boosted intake pressure and 0% EGR, and the corresponding idealized diesel cycle.

In this case, the ideal cycle thermodynamic efficiency increased by 2 percent points compared to the nonboosted case, and reached values of over 59.2%, thereby approaching the mixed cycle efficiency, but not quite reaching it. This case is much more promising as its difference with the mixed cycle is subtle, and, depending on how significant the second

order effects are, it is possible for the real isobaric cycle to achieve efficiencies similar or even higher than those of a conventional diesel cycle. The pressure at the end of the idealized cycle is 6.0 bar, and the temperature is – 405 K.

5.4 Relevant Ratios

The pressure and temperature at the end of the expansion stroke were considered for their significant role in the performance of the whole DCEE system. The higher the pressure and the temperature are at the end of the first stage of the expansion, the more energy will be available for the second stage, thereby increasing the total work output and, consequently, the efficiency of the engine. The results indicate that the isobaric cycle with a 150 bar PCP has the highest pressure at the end of expansion among the three, more than 20% higher than the mixed cycle. The temperature, however, is slightly lower, but the difference is only 4%.

Tables 5.1 and 5.2 summarize the “envelope” cycle-based pressure, cutoff and the expansion ratios. This information will help explain some of the trends presented later in the article.

	CDC			Isobaric L		Isobaric H	
	r_p	r_c	r_{exp}	r_c	r_{exp}	r_c	r_{exp}
0% EGR	1.39	1.23	13.45	1.64	10.05	1.49	11.06
17% EGR	1.39	1.27	12.95	1.67	9.90	1.51	10.90
39% EGR	1.41	1.25	13.20	1.62	10.20	1.49	11.06

Table 5.1. Pressure (r_p), cutoff (r_c), and expansion (r_{exp}) ratios of the cycles in the first set of experiments.

	CDC			Isobaric L		Isobaric H	
	r_p	r_c	r_{exp}	r_c	r_{exp}	r_c	r_{exp}
0% EGR	1.29	1.28	12.87	1.61	10.28	1.48	11.14
10% EGR	1.28	1.28	12.87	1.58	10.43	1.46	11.30
52% EGR	1.20	1.34	12.29	1.56	10.59	1.48	11.14

Table 5.2. Pressure (r_p), cutoff (r_c), and expansion (r_{exp}) ratios of the cycles in the second set of experiments.

In conclusion, the results of the theoretical cycle calculations suggest that the isobaric combustion cycle at high pressures has the ideal thermodynamic efficiency, similar to that of the mixed cycle, and having a higher exhaust pressure and temperature makes it suitable for use in the DCEE concept.

CHAPTER 6

EXPERIMENTAL RESULTS

6.1 First Set of Experiments (Low Load)

6.1.1 Thermodynamic Cycles

The in-cylinder pressure, rate of heat release and injection strategies for the first set of experiments at no-to-moderate intake boost conditions and different levels of EGR are illustrated in Figures 6.1, 6.2, and 6.3. In contrast to a CDC cycle, constant pressure combustion requires heat to be added gradually during the exhaust stroke. This results in an overall longer burn duration, which has both its advantages and disadvantages. One of the positive aspects of a slower burn are lower bulk temperatures, as demonstrated in Figure 6.4, which result in lower heat transfer losses. The drawback corresponds to a worse thermodynamic cycle in general, mainly because of a significantly lower effective expansion ratio, as seen from Table 5.1.

At different levels of EGR, the CDC and isobaric cycles demonstrated opposite trends in RoHR shapes. As the amount of EGR was increased, the heat release rate of the CDC became higher, with a shorter tail and more pressure fluctuations. On the other hand, isobaric cases had an even slower burn when the amount of EGR was raised. Such a drastic difference in trends can be explained by the different combustion modes that the two types of cycles are primarily governed by. The CDC at these conditions has a significant

premixed combustion part, while isobaric cases are predominantly governed by the diffusion flame. EGR increased the ignition delay by lowering the overall reactivity of the charge. As a result, there was more time for fuel to mix with air, making the premixed combustion prevail even more as compared to the diffusion-type combustion in the CDC case. This led to a faster burn, higher pressure ratio (rp in Table 5.1), and higher pressure rise rate, which also generated the pressure oscillations. This increase in the ignition delay can also be observed from the need for gradual advancement of the first injection timing of the CDC. In the isobaric cases however, because of a near lack of premixed combustion, the lower reactivity, caused by decreased flame temperatures and changes in air–fuel ratio, only led to longer burn durations. This might have affected the efficiency in both positive and negative ways, and is discussed later in the section.

The duration of the heat addition was also shorter for the higher-pressure isobaric cases compared to the lower ones, mainly because the injections had to be phased closer to one another to compensate for a more rapid temperature drop during the expansion stroke. This also led to a higher effective expansion ratio, as seen from Table 5.1, increasing the amount of work that can be extracted from the working fluid, and generally improving the thermodynamic efficiency.

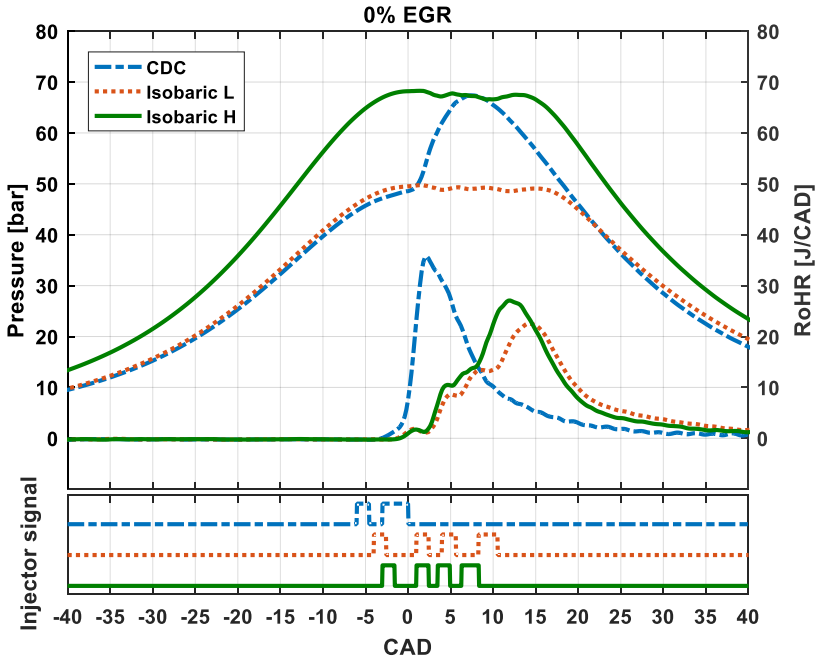

Figure 6.1. In-cylinder pressure trace, RoHR, and injector signal of the CDC, low-pressure isobaric, and high-pressure isobaric cycles with no EGR.

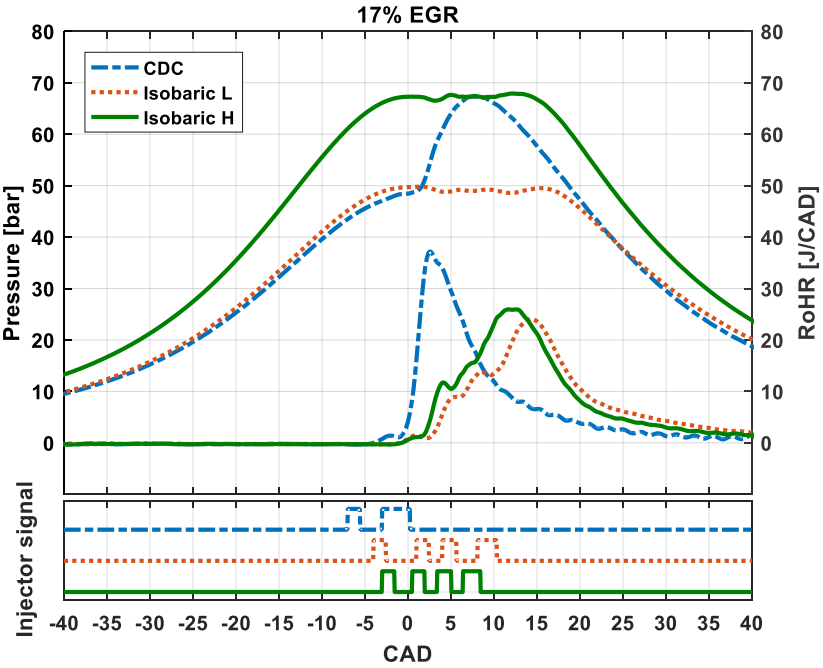

Figure 6.2. In-cylinder pressure trace, RoHR, and injector signal of the CDC, low-pressure isobaric, and high-pressure isobaric cycles with 17% EGR.

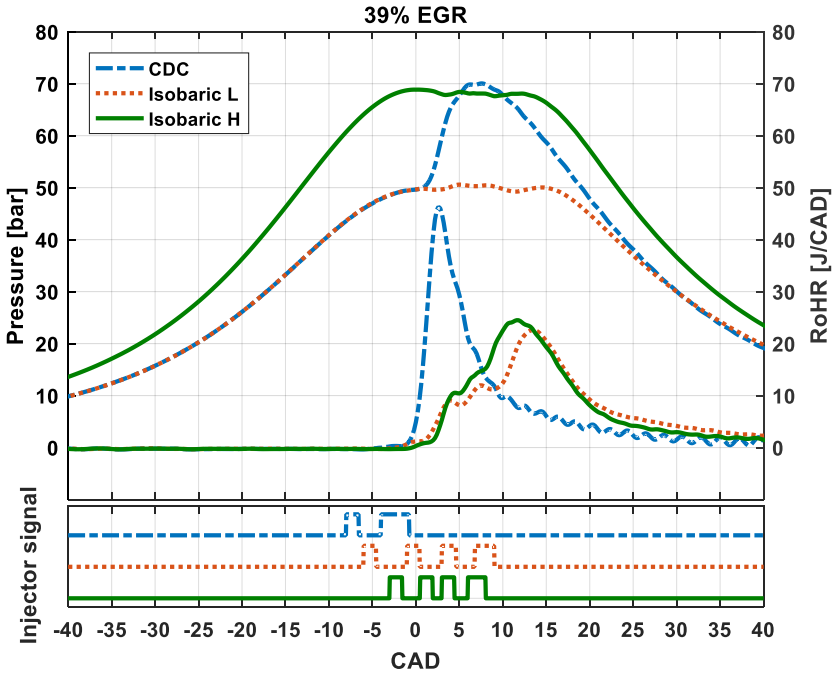

Figure 6.3. In-cylinder pressure trace, RoHR, and injector signal of the CDC, low-pressure isobaric, and high-pressure isobaric cycles with 39% EGR.

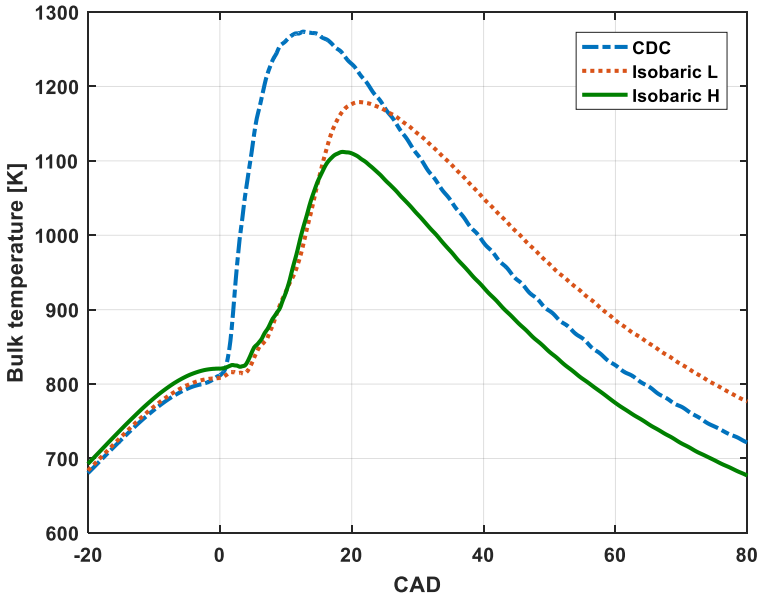

Figure 6.4. In-cylinder bulk temperature of the CDC, lower pressure isobaric, and higher pressure isobaric cycles at 0% EGR.

6.1.2 Efficiency

The combustion efficiency in all cases was between 99.7% and 99.9%. Even though the constant pressure combustion cases had, on average, slightly lower combustion efficiencies, the difference was negligible (less than 0.1%), even at low-pressure conditions. As shown later, this difference becomes even smaller at higher PCPs.

The gross indicated efficiencies of each case are presented in Figure 6.5. The error bars are based on the uncertainty in the calculations of the total amount of fuel injected per cycle, and they are within the confidence interval of 95%. It can be concluded that the isobaric combustion cycle at the same pressure level as the PCP of the CDC case, had a gross indicated efficiency approximately equal to that of the CDC cycle, at approximately 44.5%. However, the Isobaric L case had significantly lower efficiency. These results confirmed the theoretical calculations described in the previous section.

The EGR had an overall positive effect on the efficiency of all the cases. The gross indicated efficiency of the Isobaric L cycle with 39% EGR even reached the efficiency of the CDC and the Isobaric H cycles, but without EGR. The CDC case attained its highest efficiency at 17% EGR, and no further improvement was noted when more EGR was added. The efficiency of the isobaric case at higher pressure slightly exceeded that of the CDC case at 17% EGR, before reducing again at 39%. The difference in trends is explained later in the section as a part of the energy flow discussion.

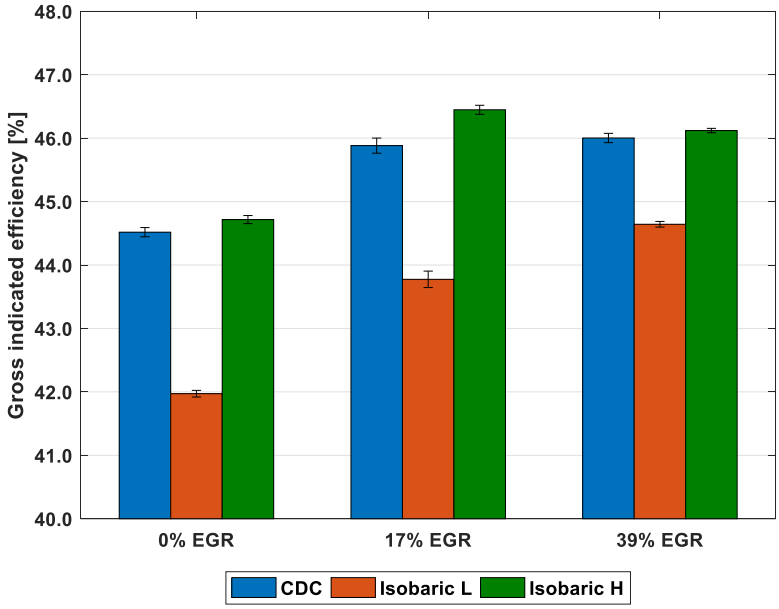

Figure 6.5. Gross indicated efficiency of the CDC, low-pressure isobaric, and high-pressure isobaric cycles at no-to-moderate boost conditions and different amounts of EGR.

6.1.3 Engine Energy Flow

The energy flow in the engine, estimated based on the methodology described in the "Real Cycle Mean Effective Pressures and Efficiency" section, is presented in Figure 6.6. The purpose of the chart is to illustrate how the energy distribution between the heat-transfer losses to the walls (i.e., HT losses) and the exhaust energy changes when different injection strategies and EGR rates are implemented. It should be noted that the combustion losses were included in the analysis, but due to their negligible magnitude compared to other losses, they are not visible on the bar chart.

It is evident that the percentage of heat going to the exhaust in the case of isobaric combustion at 50 bar (Isobaric L) is 4 percent points higher than that in the CDC case. This was caused by higher exhaust temperatures, which were measured to be 366 °C, compared to the temperature of 309 °C for the latter. This can be explained by the significantly lower effective expansion ratio of the isobaric cycle, which translates into a smaller amount of heat that can be extracted from the combustion gases until the expansion stroke is over, resulting in higher temperatures at the end of the stroke.

When boost was applied to achieve isobaric combustion at the pressure equal to the PCP of the CDC case, the exhaust energy became even more significant, i.e., over 5 percent points higher than those of the conventional cycle. The reason for the increased exhaust enthalpy is, however, different. In this case, the exhaust temperatures were significantly lower, only 288 °C. The flow rate of the gases through the exhaust system, on the other hand, was 40% higher, due to the increased pressure in the intake. The larger expansion ratio, as well as the higher lambda and lower peak cylinder temperature caused by the more diluted charge resulted in a lower temperature at the end of the cycle. This can also be observed from Figure 6.4. This difference however, was negligible compared to the large rise in the mass flow rate through the exhaust at boosted conditions causing the surge in the exhaust enthalpy (Equation 28).

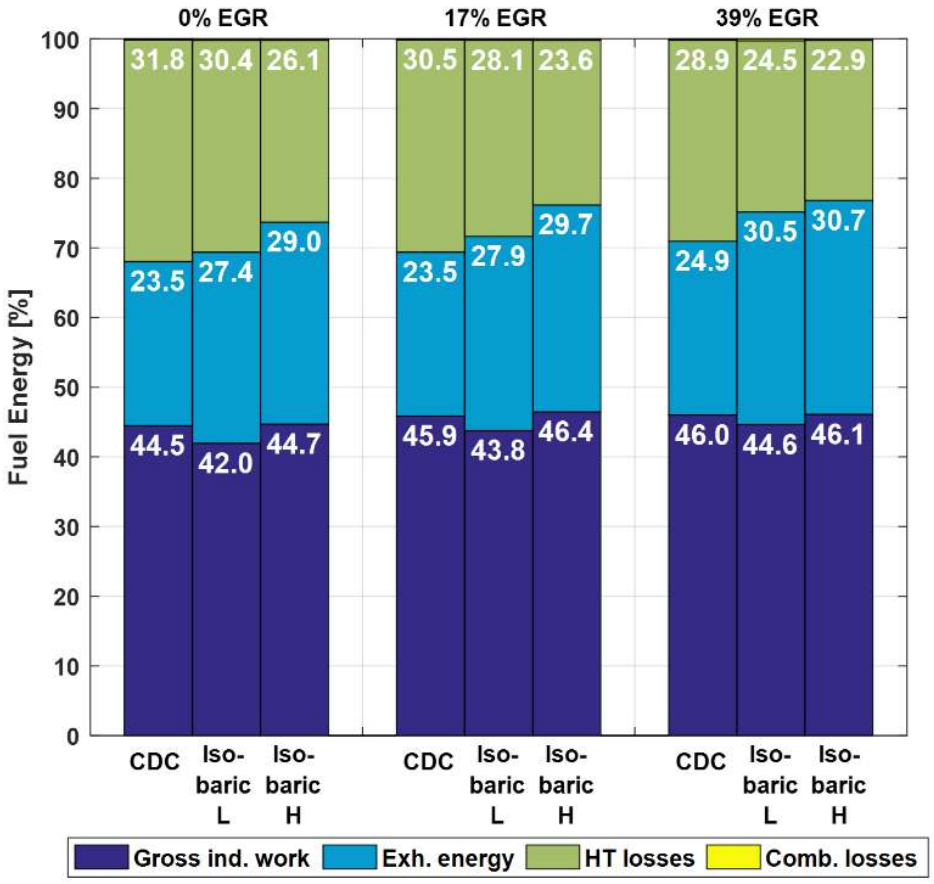

Figure 6.6. Energy distribution from the first set of experiments as a fraction of the total fuel energy in the system at different EGR rates.

The heat transfer losses to the walls followed a trend opposite to that of the exhaust energy. Both the low-pressure and high-pressure isobaric combustion cases had significantly lower heat transfer losses than the conventional cycle, due to overall lower temperatures (Figure 6.4). The reason why the Isobaric H cycle had lower bulk temperature and, consequently, lower heat transfer losses is because of higher air-fuel equivalence ratio. The trapped mass of air at boosted conditions is significantly higher compared to nonboosted conditions, the amount of fuel injected, however, is the same.

As a result, there is a larger mass of charge in the cylinder that absorbs the same amount of heat generated by combustion, leading to lower bulk temperatures.

In general, the energy distribution of the isobaric combustion cycles is more favorable for the DCEE concept, even though the higher pressure isobaric cycle is approximately at the same level as the CDC cycle in terms of the gross indicated efficiency. In the CDC case, heat transfer losses were more significant than the exhaust enthalpy, although the opposite is true for the isobaric case. This works in favor of the DCEE concept, for which it is more crucial to reduce heat losses to the walls, because the exhaust energy will be used in the expander unit and cannot be considered as losses in a conventional sense.

Next, we consider the effect of EGR on the engine energy flow. It can be seen in Figure 6.6 that the heat transfer losses consistently decreased at higher percentages of EGR, whereas the exhaust energy increased, which is, once again, beneficial for the overall efficiency of the DCEE. EGR usually has a dual effect on the efficiency of the engine. On one hand, it dilutes the in-cylinder gases with an inert gas, consisting mainly of CO2 and H2O. Both these molecules, especially water, have specific heats higher than that of air. They reduce the adiabatic flame temperature by absorbing the heat generated by the flame. This usually leads to lower bulk temperatures and reduced heat transfer losses to the walls [24]. However, this also reduces the overall reactivity and causes a degradation in the combustion process, leading to longer burn durations and less efficient thermodynamic cycle, as was mentioned in the beginning of the section. For the most part, the positive effect of EGR was prevailing in these operating conditions. The only exception was the

higher pressure isobaric case at 39% EGR, which saw a slight decrease in efficiency. However, this mild drawback was offset by the fact that the exhaust enthalpy increased, leaving more energy for the LP unit. The trend does suggest that at higher PCPs, the positive effects of EGR diminish, leading to lower thermal efficiencies. This trend is discussed in the subsequent section of the thesis.

6.1.4 Emissions

The CO, UHC, and NOx emissions were reported in the form of specific emissions, which have the units of g/kWhi. The "i" symbol indicates that these are gross indicated quantities. Soot emissions are reported as a concentration in the exhaust gas.

The isobaric combustion enabled a reduction of the NOx emissions by a factor of two. This was a direct consequence of the lower average temperatures, as seen in Figure 6.4, as well as the changes in the local equivalence ratio. It has been proved before that split injection strategies tend to reduce NOx emissions [26]. The primary reason is the sensitivity of the NOx formation mechanisms to the gas temperatures during combustion. It was shown by Zhiyu et al. [27] that it is possible to reduce NOx formation by decreasing the proportion of the fuel in the first injection while increasing it in the subsequent injections. This is a consequence of the fact that NOx emissions depend considerably on the early combustion chemistry, mainly because at this stage, the combustion products have a higher residence time at high temperatures. Isobaric heat addition, on the other hand, is characterized by primarily adding fuel late in the cycle, which enables combustion products to remain at

high temperatures for shorter durations, leading to significantly reduced NOx formation. Higher EGR rates also caused reduction in NOx emissions, again, due to lower temperatures. This is especially apparent at 39% EGR.

The CO emissions were approximately the same irrespective of the type of heat addition, and well within the EU emissions standards. Isobaric cycles had generally higher UHC emissions at all EGR rates, primarily because of the slightly lower combustion efficiency, even though the difference decreased with increase in EGR.

The soot emissions of the Isobaric H and CDC cycles were remarkably similar. However, the Isobaric L cases demonstrated higher values, especially at higher rates of EGR. This was caused by a significantly higher equivalence ratio (lower lambda), which led to the fuel being starved of oxygen, thereby forming carbon instead of CO2. In the CDC case, this trend was not observed because the temperatures and residence time of the combustion products are much higher, allowing the formed soot to oxidize before the end of the cycle. The Isobaric H case never reached equivalence ratios as high as the Isobaric L did; thus, the soot production did not increase significantly.

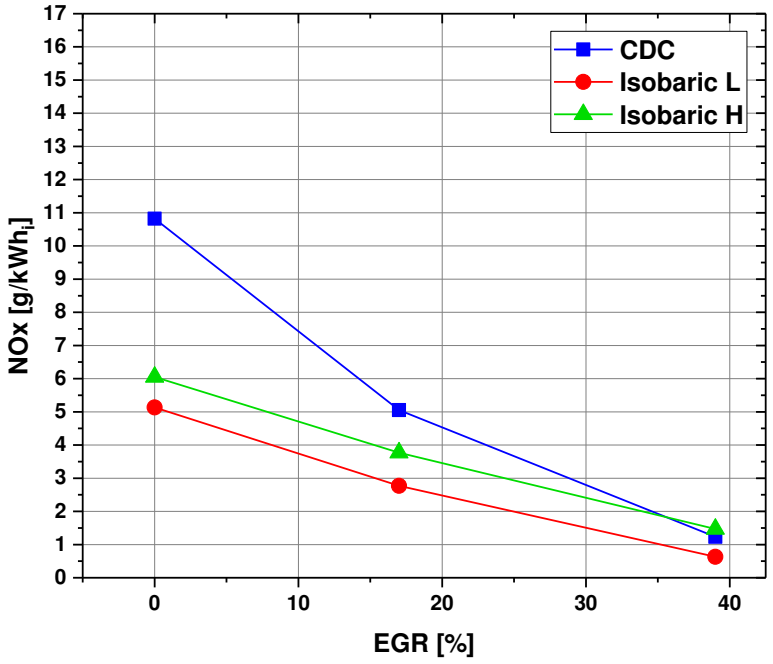

Figure 6.7. Gross specific NOx emissions as a function of EGR % for the first set.

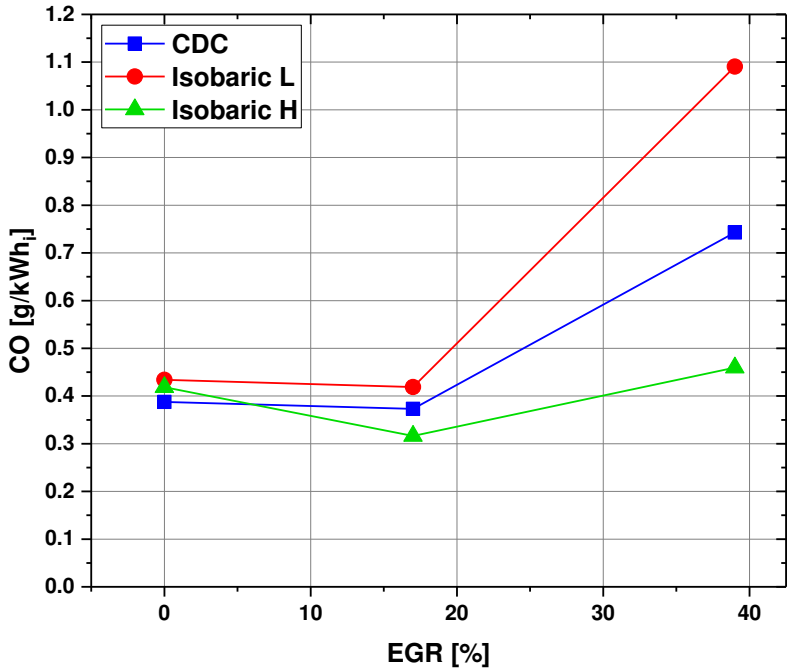

Figure 6.8. Gross specific CO emissions as a function of EGR % for the first set.

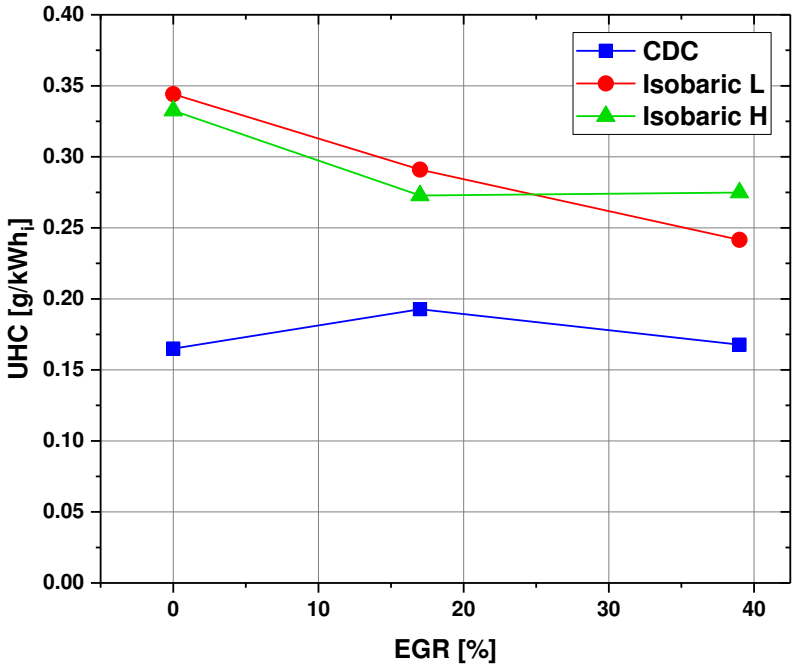

Figure 6.9. Gross specific UHC emissions as a function of EGR % for the first set.

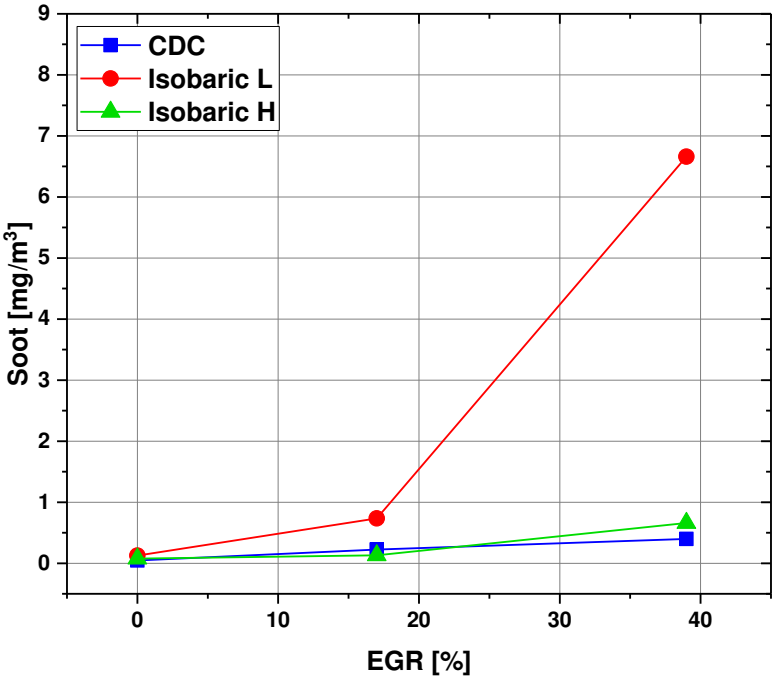

Figure 6.10. Exhaust soot concentration as a function of EGR % for the first set.

6.2 Second Set of Experiments (High Load)

6.2.1 Thermodynamic Cycles

As in the previous low-pressure cases, to achieve isobaric combustion at 150 bar, the injections were required to be spaced even tighter, leading to overall shorter burn durations.

It can also be concluded that at high loads, and pressure levels in the cylinder approaching 150 bar, the differences between the heat release rate shapes of different modes of combustion become less apparent. In particular, when the injection duration of the CDC case was increased to allow higher IMEPs, the shape of the heat release rate approached that of the isobaric cases (Figures 6.11, 6.12, 6.13). This effectively implies a smaller isochoric part of the heat addition process, which reduces the advantage of a conventional mixed cycle compared to an isobaric cycle. However, the drawbacks of the CDC still persist, which result in a lower thermodynamic efficiency. The EGR also affected both types of power cycles in a similar way, in contrast to the results from the first set of the experiments. This is also caused by lower significance of the isochoric part (premixed combustion), and the overall tendency of the CDC to approach the isobaric cycles. In an extreme case, when 52% of EGR was used, the CDC cycle had such a slow burn that the inlet pressure had to be increased so that the PCP of 150 bar could be reached while maintaining the same fuel consumption. This was the reason why the peak motored pressure of the CDC at 52% EGR was higher than that of the Isobaric L case, as seen in Figure 6.13. However, this did not affect the trends in efficiency and energy balance, as shown later in the section.

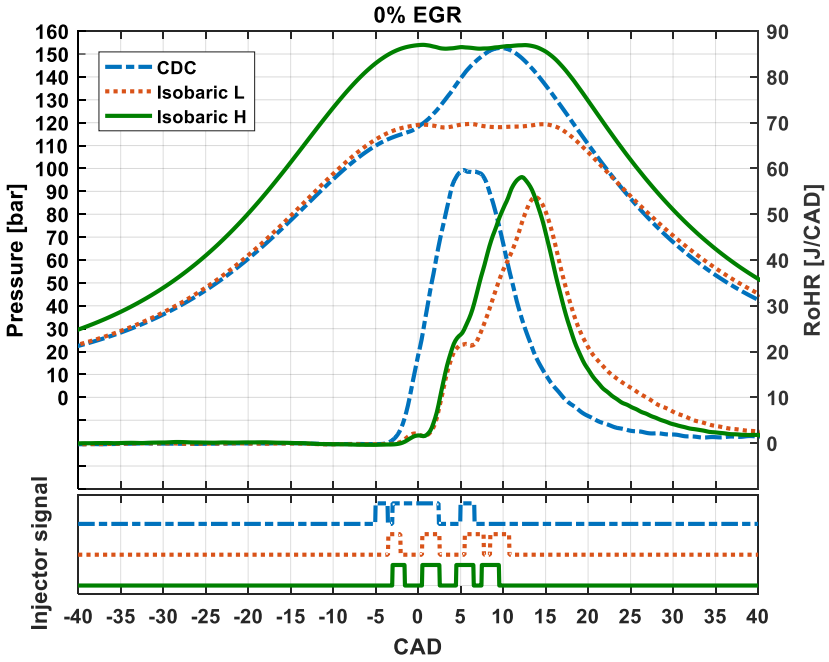

Figure 6.11. In-cylinder pressure trace, RoHR, and injector signal of the CDC, low-pressure isobaric, and high-pressure isobaric cycles with no EGR.

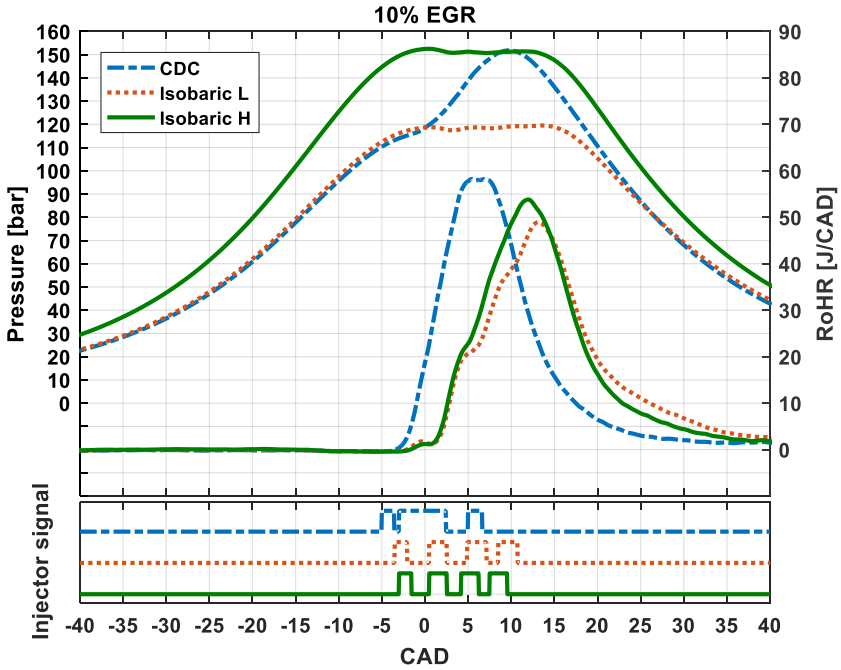

Figure 6.12. In-cylinder pressure trace, RoHR, and injector signal of the CDC, low-pressure isobaric, and high-pressure isobaric cycles with 10% EGR.

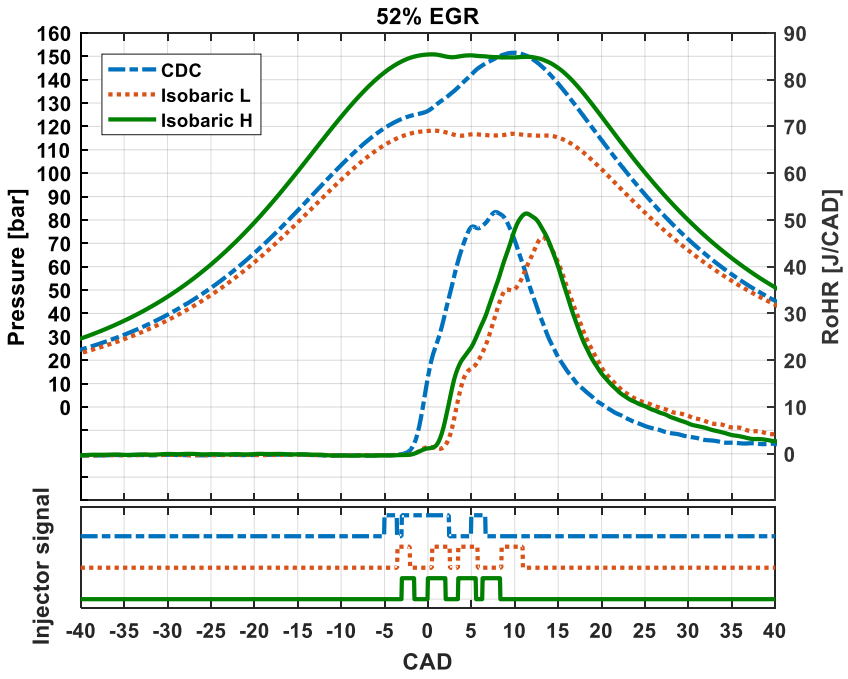

Figure 6.13. In-cylinder pressure trace, RoHR, and injector signal of the CDC, low-pressure isobaric, and high-pressure isobaric cycles with 52% EGR.

6.2.2 Efficiency

The combustion efficiency in all the cases was between 99.8% and 99.9%, and the difference between the CDC and Isobaric cases was negligible.

The gross indicated efficiency that was achieved with the constant pressure combustion at 150 bar slightly exceed that of the CDC case reaching almost 49.5% at 0-EGR conditions (Figure 6.14). The Isobaric L cycle had an efficiency lower by almost 2 percent-points. When EGR was introduced however, the Isobaric L reached efficiencies comparable to those of the CDC and Isobaric H, which is the same trend as in the first set of the

experiments. The Isobaric H cycle, on the other hand, exhibited consistently decreasing efficiency as more EGR was added. This trend is somewhat different from the one observed at lower pressures, where the gross indicated efficiency of the Isobaric H case first increased at medium rates of EGR and then slightly decreased at higher rates. This can, once again, be explained by the dual nature of EGR. At higher pressure levels, the benefits from decreasing the flame temperature are set back by its tendency to degrade the combustion process. This trend is visualized in Figure 6.15.

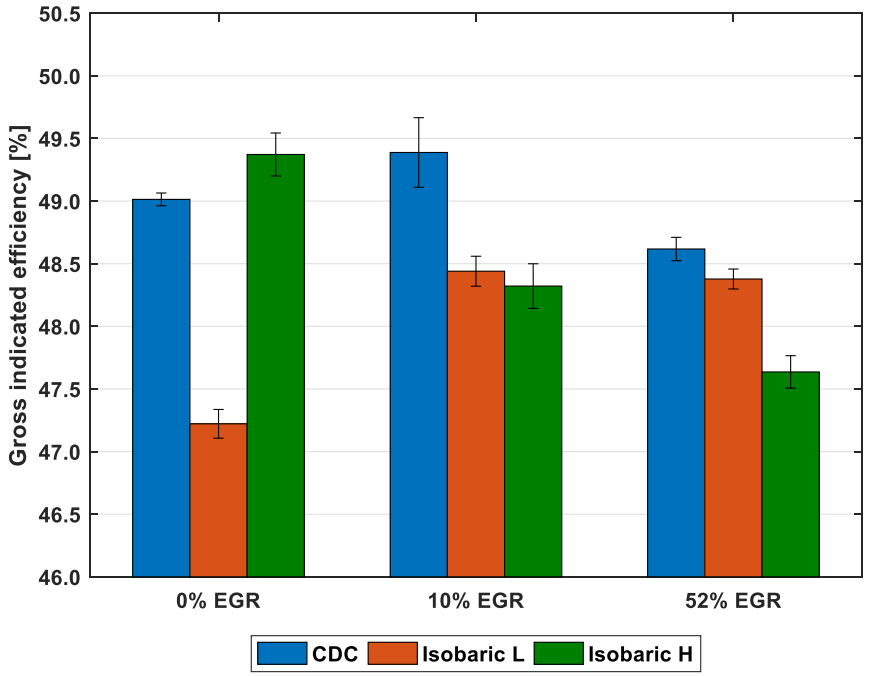

Figure 6.14. Gross indicated efficiency of the CDC, low-pressure isobaric, and high-pressure isobaric cycles at high-boost conditions and different amounts of EGR.

6.2.3 EGR and PCP

To clearly observe the relation between the effects of EGR and PCP, the air–fuel equivalence ratio (lambda) and the fraction of HT losses at different PCPs were plotted as a function of the EGR rate. Next, a first order polynomial was fit onto the data, and the slope of each line was computed. These slopes are effectively the derivatives of the HT loss fraction and the lambda with respect to the fraction of EGR in the intake air, and can be expressed as $\frac{dHT_{loss}}{dEGR}$ and $\frac{d\lambda}{dEGR}$, respectively. These derivatives were plotted and are shown in Figure 6.15 as a function of the PCP. It should be noted that all the values are negative, indicating once again that the HT loss and lambda are both inversely proportional to the rate of EGR. However, these quantities follow opposite trends with respect to the PCP. It is evident that the magnitude of $\frac{d\lambda}{dEGR}$ increases at higher pressures. This means that at higher PCPs, the reduction in air–fuel equivalence ratio is faster, leading to richer mixtures and more degraded combustion process at the same rates of EGR, compared to lower PCPs. Moreover, the fuel burns later in the cycle, where the area of the liner exposed to the high temperature gases is much larger, thereby leading to higher heat transfer losses and a decrease in the thermodynamic efficiency. This can also be observed from the HT loss percentage shown in Figure 6.16. On the other hand, the tendency of the EGR to decrease the heat transfer losses via reduced flame temperatures becomes less pronounced with increase in the PCP. It can be seen in Figure 6.15 that the magnitude of $\frac{dHT_{loss}}{dEGR}$ decreases significantly, reaching values very close to 0, suggesting that as the PCP is increased, the positive effect of EGR is diminished. This leads to a completely different

trend corresponding to the response of efficiency to the added EGR at different PCPs. Similar behavior was also observed by Timothy et al. in their investigation of the impact of EGR on the HD diesel engine performance [25].

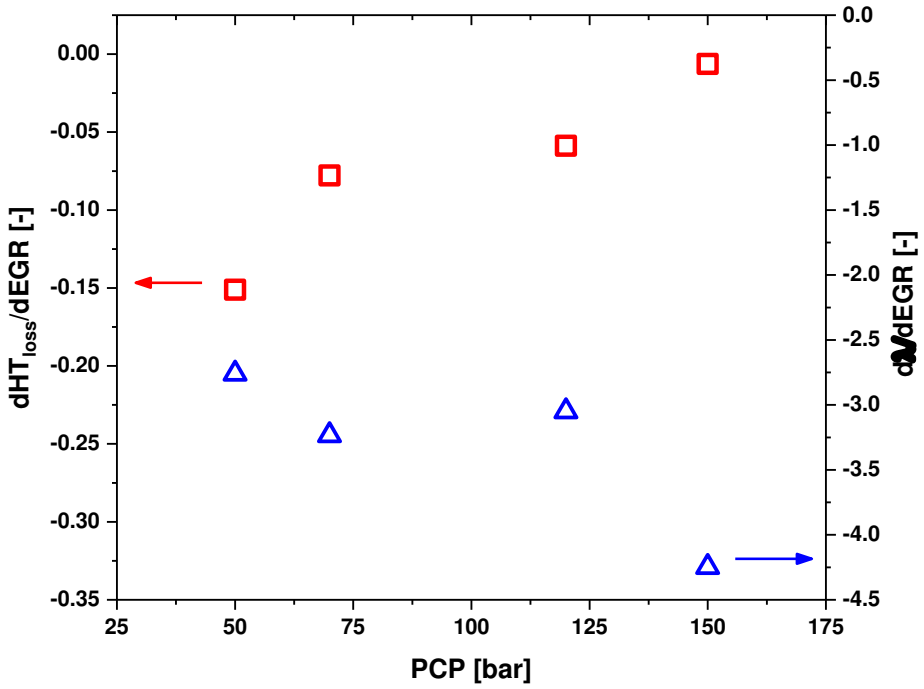

Figure 6.15. Derivatives of the air–fuel equivalence ratio (lambda) and heat transfer losses (HT loss) of the isobaric cycles with respect to the EGR rate as a function of the peak cylinder pressure (PCP). Squares correspond to the left axis, triangles correspond to the right axis.

It should be noted that the derivatives did not undergo significant change between the 70 bar- and 120 bar-PCP cases because the amount of fuel injected per cycle was changed between the first and second sets of experiments. This caused the combustion deterioration to reset slightly; however, the trend still persisted. Even though at higher EGR rates, the effective expansion ratio is slightly higher for the isobaric cases, as seen from Table 5.2,

this does not imply that the thermodynamic cycle is better overall. Because the rate of heat release from each injection was lower with EGR, the injections had to be phased closer to each other, leading to a shorter duration in which the pressure was kept constant, thereby increasing the expansion ratio. However, the amount of heat released during the descending part of the RoHR trace caused higher HT losses, because of the larger exposed area of the liner. At 150 bar PCP, this trend is still not as pronounced as it is expected to be at the target pressures of the DCEE concept, i.e., at approximately 300 bar.

6.2.4 Engine Energy Flow

The energy flow in the system at 150 bar peak pressures, depicted in Figure 6.16, differs significantly from that for the first set of experiments at lower pressures. First, the fraction of exhaust energy is significantly higher for the high-pressure cases, which also means that less energy is lost to the cylinder walls through heat transfer. However, the overall trends between the CDC and isobaric cycles are similar. On the other hand, the effect of EGR, as was described in the previous paragraph, was much more ambiguous. High EGR rates were still beneficial for the Isobaric L case, but they had a mixed effect on the Isobaric H case. The amount of energy that transformed to useful work decreased, while the exhaust energy increased. A detailed analysis of the complete DCEE model is required to be able to clearly see the impact on the overall efficiency of the system. It can be concluded, however, that at the target pressures of the DCEE (~300 bar), EGR would potentially have more negative than positive impacts on the efficiency of the engine.

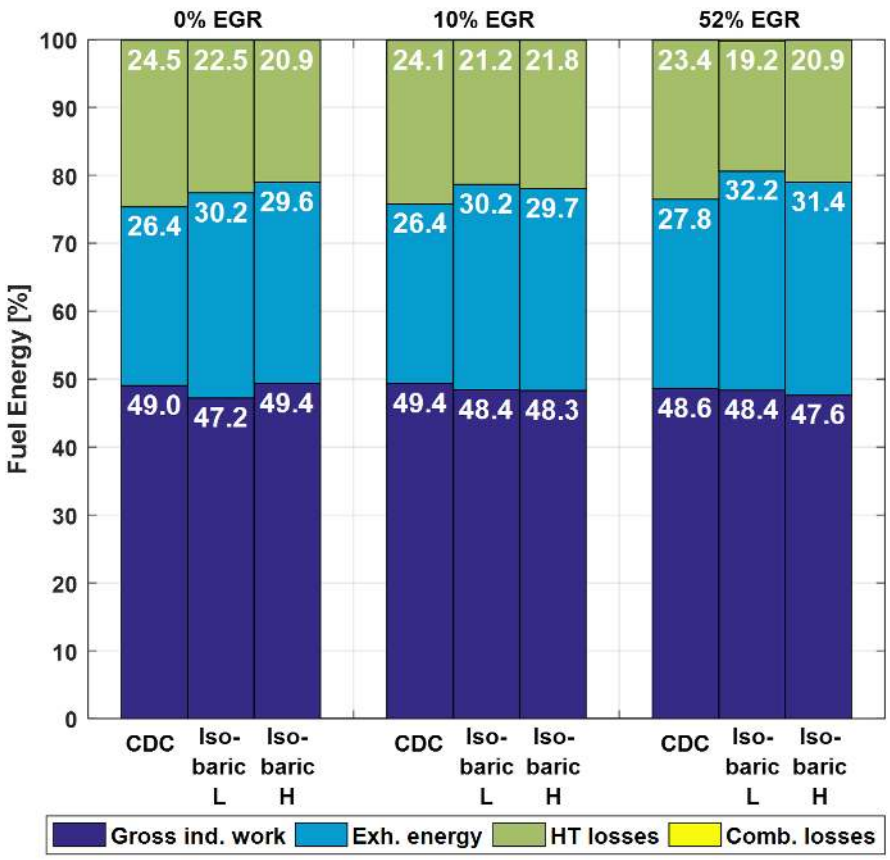

Figure 6.16. Energy distribution from the second set of experiments as a fraction of the total fuel energy in the system at different EGR rates.

Nevertheless, the trends do indicate the existence of a "sweet spot", where the PCP and EGR rate are optimized for best efficiency. Finding this operating point will require a parametric study, which is beyond the scope of this study.

Currently, the trend is to utilize very high EGR rates to minimize NOx emissions and, potentially, eliminate the need for NOx after-treatment. One of the important results of this study is the fact that the Isobaric L case approached, in terms of the gross indicated efficiency, the CDC case at high EGR rates. This means that an isobaric cycle with significantly lower peak cylinder pressure can be used instead of a conventional diesel

cycle, without sacrificing thermal efficiency, in scenarios where high EGR rates are required. The benefit of using an isobaric cycle in that case would involve reduced friction losses due to lower PCPs, as well as lower heat transfer losses. The difference between the friction losses of the CDC and Isobaric L cases was estimated from the engine brake power data according to Equation 34. The resultant difference in FMEPs is 0.57 bar, which is approximately 2.5% of the total fuel energy and cannot be neglected.

6.2.5 Emissions

At the peak pressures close to 150 bar, the CO and UHC emissions generally reduced. This was because of not only the slightly lower equivalence ratio but also the increased kinetic rates as a consequence of higher molecular number densities [28]. The same trend was observed by Koci et al. [29].

The isobaric cycle at the pressure level equal to that of the CDC had CO, UHC, and soot emissions approximately equal to those of the CDC case. The magnitude of NOx, however, was almost two times lower, as in the first experimental set. The constant pressure combustion case at lower pressure, in contrast to the first set, had the lowest CO and UHC emissions of the three cases. A 10% EGR caused a slight decrease in the NOx and the soot emissions. At 50% EGR however, the NOx values reduced to approximately 0.5 g/kWh, and in the case of the Isobaric L cycle, this value reduced to 0.3 g/kWh, which is in compliance with the EU regulations. Soot emissions increased only for the lower isobaric case, because of the lower lambda, as discussed previously; however, the soot emissions remained at approximately the same level for the other two cycles.

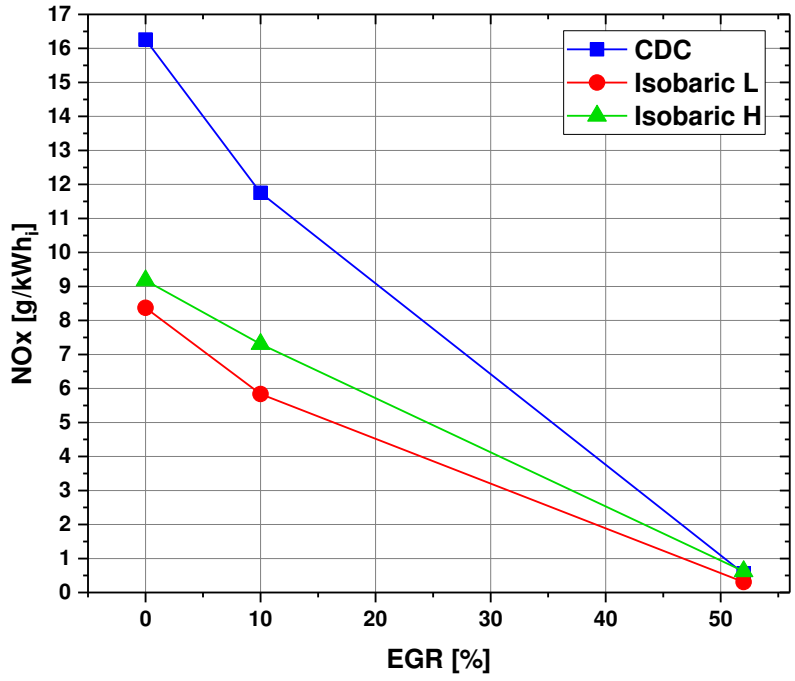

Figure 6.17. Gross specific NOx emissions as a function of EGR % for the second set.

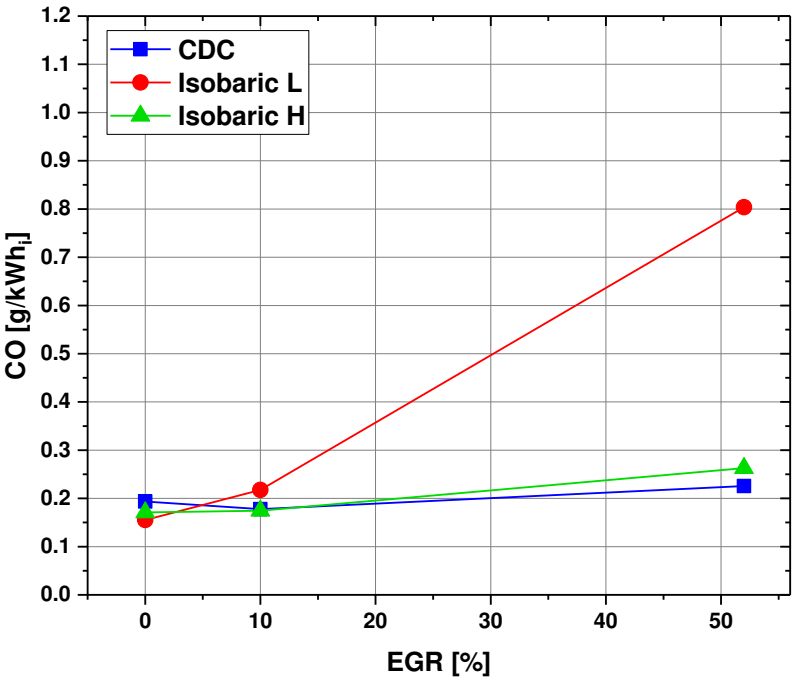

Figure 6.18. Gross specific CO emissions as a function of EGR % for the second set.

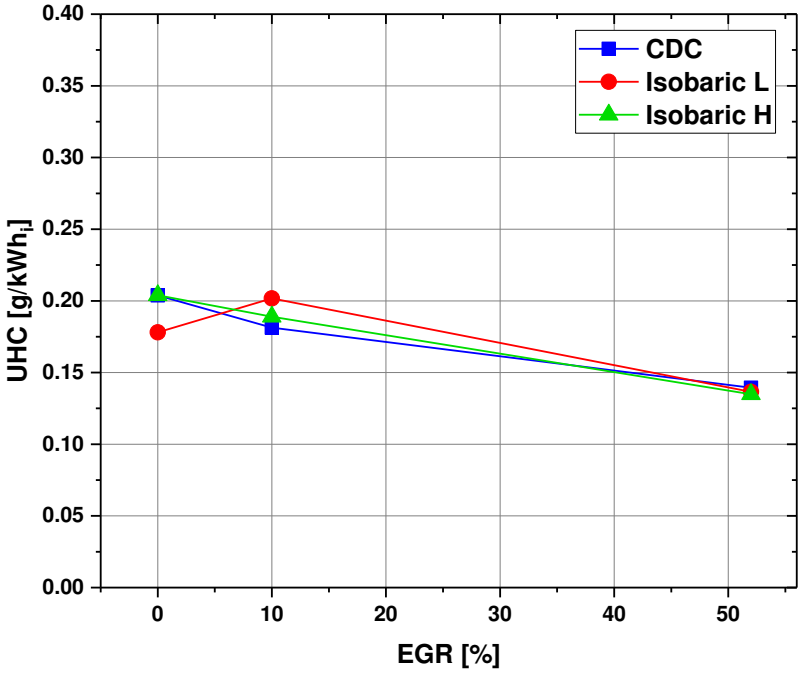

Figure 6.19. Gross specific UHC emissions as a function of EGR % for the second set.

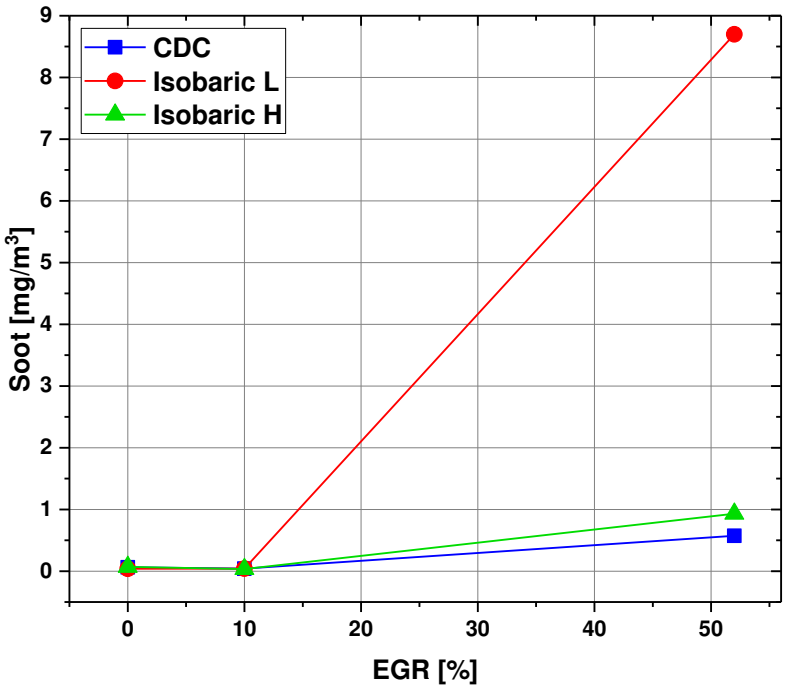

Figure 6.20. Exhaust soot concentration as a function of EGR % for the second set.

CHAPTER 7

PRACTICAL CHALLENGES ASSOCIATED WITH ISOBARIC HEAT ADDITION

It is expected to be more difficult to achieve not only high quality isobaric heat addition (low waviness) but also an isobaric cycle in general as the in-cylinder pressure levels are raised. This is because of both the enhanced reactivity and a higher rate of pressure and temperature drop due to expansion, which require each injection to be initiated closer to the end of the previous injection. In some cases, this process resulted in the inability of the injector to complete the needle motion and stop the flow before the start of the next injection, which led to a merging of two shots and general instability of the injection system. As an example, the injection strategy of the isobaric cycle with 150 bar PCP and 0% EGR can be considered. The following calculations are approximate but provide a clear understanding of the situation.

In the abovementioned case, the third injection occurred at 4.5 CAD ATDC with an injection duration of 280 µs, which corresponds to 2.0 CAD at the engine speed of 1200 RPM. This means that the injection event is expected to finish at 6.5 CAD ATDC. The next signal is sent at 7.5 CAD ATDC, allowing a gap of only 1.0 CAD between two shots. The F2E distributed pump common rail system (DPCRS) used in this study is capable of delivering multiple injections with a 200 µs separation between shots [30], which corresponds to 1.44 CAD at 1200 RPM. This indicates that the required separation between two injections is shorter than the minimum shot-to-shot separation that the system is rated

for, leading to instabilities. An example of the rate trace obtained from the fuel injection system used in the current study is illustrated in Figure 7.1

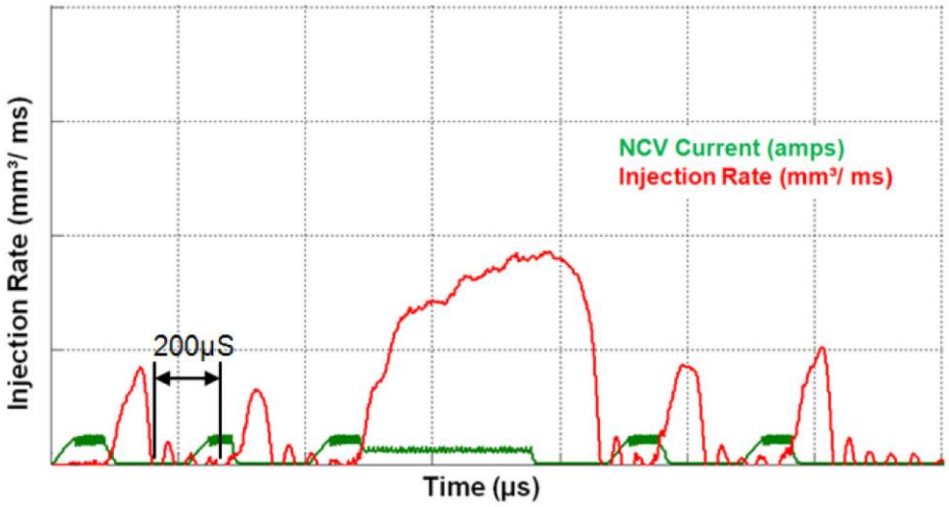

Figure 7.1 Rate Trace Example of Five Injection Events of the F2E DPCRS [30].

The next logical step was to investigate if a higher fuel injection rate could enable longer gaps between injections via reduced injection durations, while maintaining constant pressure combustion. Hence, the rail pressure was increased up to 2300 bar and another isobaric cycle at 150 bar PCP was recorded. All the other parameters were kept the same as in the first case, including the total amount of fuel mass injected. The pressure trace, RoHR, and injector signal of the 150 bar-PCP isobaric cycles with 1500 bar and 2300 bar rail pressures (RP) are presented in Figure 7.2.

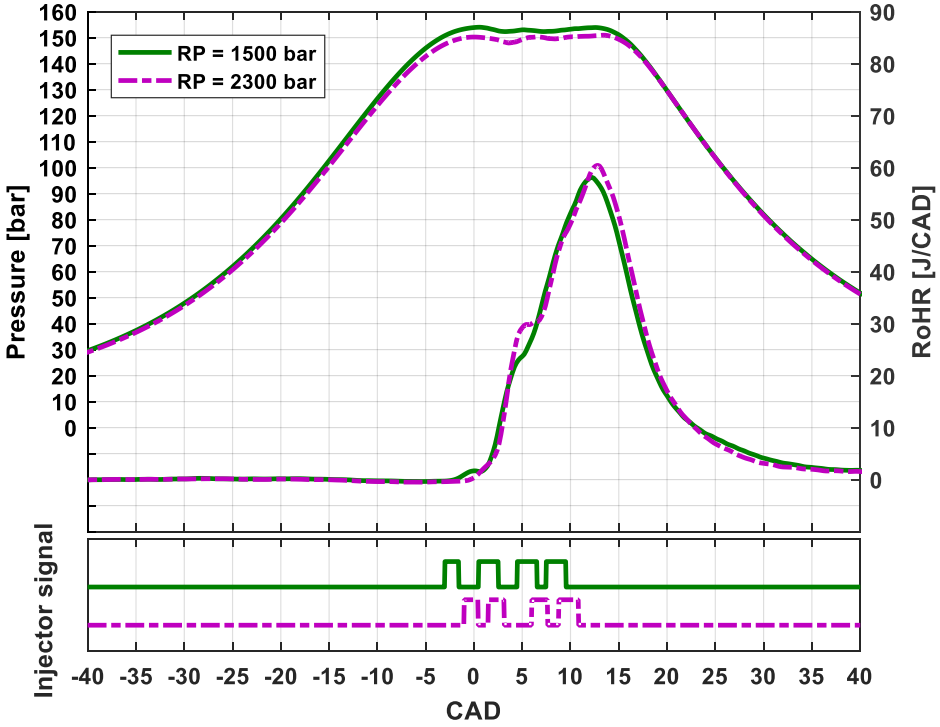

Figure 7.2. In-cylinder pressure trace, RoHR, and injector signal of the isobaric combustion cycles with 1500 bar and 2300 bar common rail pressures and no EGR.

At first glance, the results appear counterintuitive. A higher injection pressure generally did not lead to longer shot-to-shot separations. It even caused a shorter gap between the first and second injections. The reason behind this behavior is that increased injection rates not only reduced the injection durations but also enhanced the fuel atomization, leading to a better mixing and shorter burn duration from each shot. This resulted in the need to phase the injections close to one another to maintain constant pressure combustion.

These results suggest that if a constant pressure combustion is required at a pressure higher than 150 bar, solenoid valve injectors, similar to the ones used in the experimental

campaign described in this thesis, would not be suitable. Instead, piezoelectric fuel injectors with higher needle speeds should be used.

The injection durations are limited as well. Because the ignition delays at high pressures are smaller, the premixed combustion becomes insignificant, leading to little-to-no increase in pressure from each injection as the injection duration is further increased. As a result, higher IMEPs cannot be easily realized by increasing the duration of each injection under the constraints of an isobaric heat addition. The conclusion is that, to be able to achieve IMEPs higher than those considered in this work (~11 bar) at 150 bar PCP, either the number of injections must be increased to more than 4, or a more wavy pressure trace during combustion must be implemented. The latter option, however, will probably lead to lower thermodynamic efficiency.

CHAPTER 8

SUMMARY AND FUTURE WORK

8.1 Summary/Conclusions

This study investigated the effects of different injection strategies and different rates of EGR on the engine thermal efficiency and emissions. Experiments were performed on a single cylinder HD engine. Near isobaric combustion was studied at different peak cylinder pressures and EGR rates and compared to conventional diesel combustion. In summary, the study demonstrates the following:

- An isobaric combustion cycle can be achieved with a conventional fuel injection system by using multiple consecutive injections.
- Isobaric combustion and conventional diesel combustion cycles have approximately equal gross indicated efficiencies at the same peak cylinder pressures and no external EGR.
- Isobaric cycles have lower heat transfer losses than the conventional diesel combustion cycles, because of their lower average in-cylinder temperatures and higher exhaust energy, mainly owing to the lower effective expansion ratio. This makes isobaric cycles suitable for use in the DCEE concept.
- The combustion efficiency is not impacted by the isobaric heat addition and, irrespective of the type of the cycle, remains above 99.7%.

- Increase in the peak cylinder pressure generally leads to the increase in the gross indicated efficiency for both conventional diesel combustion and isobaric combustion cycles. The magnitude of the increase is also similar.
- In the majority of the scenarios considered in this study, higher EGR rates caused a decrease in the heat transfer losses, while increasing the exhaust energy. However, as the peak cylinder pressures were increased, EGR's positive effect on the heat transfer losses started to diminish, while the trend with the exhaust energy persisted. As a result, a reduction in the gross indicated efficiency with higher EGR rates was observed at peak cylinder pressures approaching 150 bar. The trends suggest that it is possible to optimize the peak cylinder pressure and the EGR rate to achieve higher efficiencies.
- If high EGR rates are required, an isobaric cycle with significantly lower peak cylinder pressure can still be used instead of a conventional diesel cycle, without sacrificing the thermal efficiency. In such a case, the isobaric combustion has the benefit of lower friction losses due to lower PCPs, in addition to lower heat transfer losses.
- The NOx emissions are approximately two times lower for the isobaric combustion cycle compared to the conventional diesel cycle. The CO, UHC and soot emissions of the isobaric combustion and conventional diesel combustion cycles are generally similar.
- At peak cylinder pressures above 150 bar, more fuel is required to be injected, and shorter durations must be set between the multiple injections. Hence, it is expected

to be challenging to achieve constant pressure combustion using conventional solenoid fuel injectors.

8.2 Future Work

The research work presented in this thesis can be further extended by performing three-dimensional numerical simulations. The results of the simulations shall provide detailed information of the spray-to-spray interaction and its effect on the heat release rate shape and pollutant formation. Furthermore, trends in HT transfer losses are expected to be better understood with spatially resolved in-cylinder temperature data, which simulations can provide. An example of the geometry, which represents the engine used in this thesis is presented in Figure 8.1. It includes the combustion chamber, enclosed by the liner (green), piston (red), cylinder head (brown) and valve bottom surfaces. In addition, the inlet (blue) and exhaust (white) ports will also be modeled to provide realistic boundary conditions in the combustion chamber.

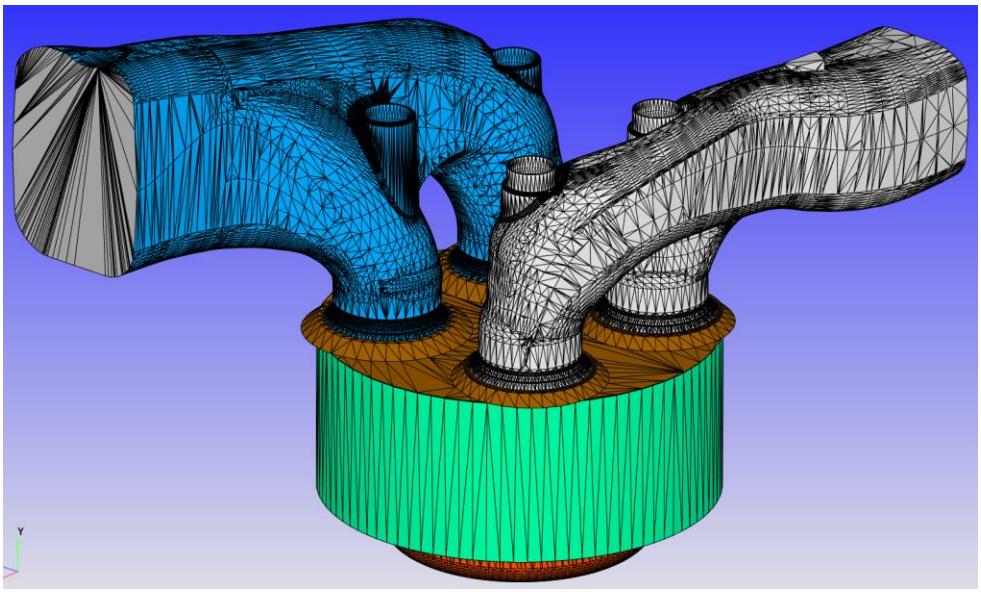

Figure 8.1. The combustion chamber, and inlet and exhaust ports surface geometry to be used in three-dimensional numerical simulations.

Furthermore, the compressor and expander units, as well as the ports that connect them to the combustor unit of the DCEE concept, can also be modeled in 3-D to extend upon the 1-D GT-Power simulations that have already been performed [11-14].

Another technology to be studied in the future is the system of three injectors, similar to what Okamoto and Uchida implemented in their work [15]. Such a system can provide a greater flexibility in the rate of heat release shaping, potentially reduce energy losses via heat transfer, thus further increasing the thermal efficiency of the engine, and minimize formation of certain pollutants. An illustration of such a system is presented in Figure 8.2.

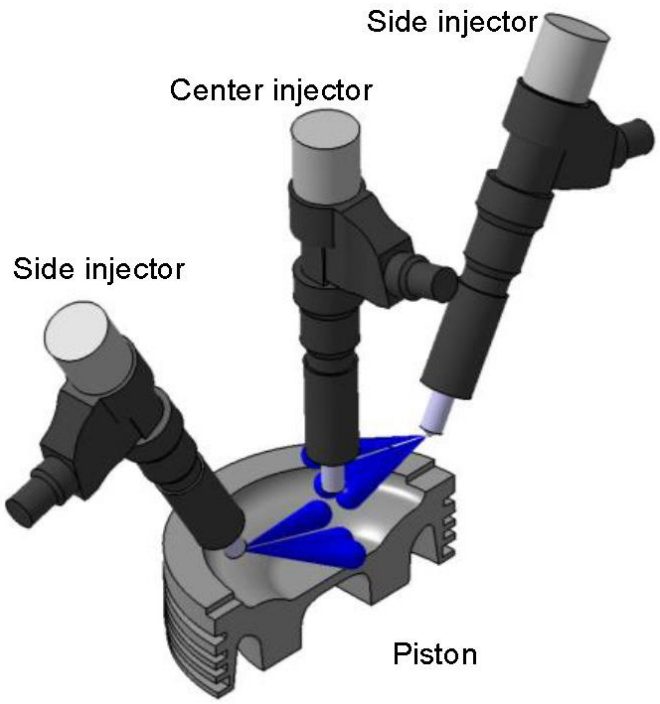

Figure 8.2. The system of three injectors by Uchida et al. with the spray orientation in blue [15].

BIBLIOGRAPHY

1. Allen, Myles R., Vicente R. Barros, John Broome, Wolfgang Cramer, Renate Christ, John A. Church, Leon Clarke et al. "IPCC fifth assessment synthesis report-climate change 2014 synthesis report." (2014).

2. https://www.epa.gov/ghgemissions/inventory-us-greenhouse-gas-emissions-and-sinks-1990-2016.

3. European Commission, Strategy for reducing heavy-duty vehicles' fuel consumption and CO2 emissions, 2014. http://ec.europa.eu/clima/policies/transport/vehicles/heavy/docs/com_285_2014_en.pdf

4. ExxonMobil. The outlook for energy: A view to 2040. 2016.

5. Muncrief, R., and B. Sharpe. "Overview of the heavy-duty vehicle market and CO2 emissions in the European Union." International Council on Clean Transportation Working Paper (December) (2015): 1-14.

6. http://s04.static-shell.com/content/dam/shell-new/local/country/deu/downloads/pdf/publications-2010truckstudyfull.pdf

7. https://www.gov.uk/government/uploads/system/uploads/attachment_data/file/479143/rfs0141.xls

8. Phillips, F., Gilbert, I., Pirault, J.-P., and Megel, M., Scuderi Split Cycle Research Engine: Overview, Architecture and Operation. SAE Int. J. Engines, 2011. 4(1)

9. Clarke, J. and O'Malley, E., “Analytical Comparison of a Turbocharged Conventional Diesel and a Naturally Aspirated Compact Compression Ignition Engine both Sized for a Highway Truck,” SAE Technical Paper 2013-01-1736, 2013, doi:10.4271/2013-01-1736.

10. https://ricardo.com/news-and-media/press-releases/game-changing-ricardo-concept-for-high-efficiency

11. Lam, N., Tuner, M., Tunestal, P., Andersson, A. et al., "Double Compression Expansion Engine Concepts: A Path to High Efficiency," SAE Int. J. Engines 8(4):1562-1578, 2015, https://doi.org/10.4271/2015-01-1260.

12. Lam, Nhut, Arne Andersson, and Per Tunestal. "Double Compression Expansion Engine Concepts: Efficiency Analysis over a Load Range." SAE Technical Papers 2018 (2018).

13. Bhavani Shankar, V., Lam, N., Andersson, A., and Johansson, B., "Optimum Heat Release Rates for a Double Compression Expansion (DCEE) Engine," SAE Technical Paper 2017-01-0636, 2017, doi:10.4271/2017-01-0636.

14. Shankar, Bhavani, Vijai Shankar, Bengt Johansson, and Arne Andersson. "Double Compression Expansion Engine: A Parametric Study on a High-Efficiency Engine Concept." SAE Technical Paper Series (2018).

15. Okamoto, T. and Uchida, N., "New Concept for Overcoming the Trade-Off between Thermal Efficiency, Each Loss and Exhaust Emissions in a Heavy Duty Diesel Engine," SAE Int. J. Engines 9(2):2016, doi:10.4271/2016-01-0729.

16. Heywood, John B. "Internal combustion engine fundamentals." (1988).

17. Johansson, Bengt. Combustion Engines. Department of Energy Sciences, Lund University, 2014.

18. Dernotte, J., Dec, J., and Ji, C., "Energy Distribution Analysis in Boosted HCCI-like / LTGC Engines - Understanding the Trade Offs to Maximize the Thermal Efficiency," SAE Int. J. Engines 8(3):2015, doi:10.4271/2015-01-0824.

19. Woschni, Gerhard. A universally applicable equation for the instantaneous heat transfer coefficient in the internal combustion engine. No. 670931. SAE Technical paper, 1967.

20. Gatowski, J. A., En N. Balles, K. M. Chun, F. E. Nelson, J. A. Ekchian, and John B. Heywood. Heat release analysis of engine pressure data. No. 841359. SAE Technical paper, 1984.

21. http://mesaengine.com/

22. Manente, V., Johansson, B., Tunestal, P., and Cannella, W., “Effects of Different Type of Gasoline Fuels on Heavy Duty Partially Premixed Combustion,” SAE Int. J. Engines 2(2):71-88, 2010, doi:10.4271/2009- 01-2668.

23. O'Connor, J. and Musculus, M., "Post Injections for Soot Reduction in Diesel Engines: A Review of Current Understanding," SAE Int. J. Engines 6(1):2013, doi:10.4271/2013-01-0917.

24. Ladommatos, N., S.M. Abdelhalim, H. Zhao, and Z. Hu, “The Dilution, Chemical, and Thermal Effects of Exhaust Gas Recirculation on Diesel Engine Emissions – Part 3: Effects of Water Vapour”, SAE Paper 971659, International Spring Fuels and Lubricants Meeting, Dearborn, Michigan, 1997.

25. Jacobs, Timothy, Dennis N. Assanis, and Zoran Filipi. The impact of exhaust gas recirculation on performance and emissions of a heavy-duty diesel engine. No. 2003-01-1068. SAE Technical paper, 2003.

26. Nehmer, Daniel A., and Rolf D. Reitz. "Measurement of the effect of injection rate and split injections on diesel engine soot and NOx emissions." SAE transactions (1994): 1030-1041.

27. Han, Zhiyu, Ali Uludogan, Gregory J. Hampson, and Rolf D. Reitz. "Mechanism of soot and NOx emission reduction using multiple-injection in a diesel engine." SAE transactions 105 (1996): 837-852.

28. Colban W. F., Miles P. C., Oh S., “Effect of Intake Pressure on Performance and Emissions in an Automotive Diesel Engine Operating in Low Temperature Combustion Regimes”, SAE Paper 2007-01-4063, 2007.

29. Koci, C., Ra, Y., Krieger, R., Andrie, M. et al., "Multiple-Event Fuel Injection Investigations in a Highly-Dilute Diesel Low Temperature Combustion Regime," SAE Int. J. Engines 2(1):837-857, 2009, https://doi.org/10.4271/2009-01-0925.

30. Meek, G., Williams, R., Thornton, D., Knapp, P. et al., "F2E - Ultra High Pressure Distributed Pump Common Rail System," SAE Technical Paper 2014-01-1440, 2014, doi:10.4271/2014-01-1440.

APPENDICES

Appendix A

Mean Effective Pressure in the Two Sets of Experiments

	First set of experiments								
	NO EGR			MIN EGR[1]			MAX EGR[2]		
	CDC	Isobaric L	Isobaric H	CDC	Isobaric L	Isobaric H	CDC	Isobaric L	Isobaric H
FuelMEP	10.29	11.14	11.09	10.84	11.29	11.21	10.88	10.87	10.62
HTMEP	3.27	3.39	2.89	3.30	3.18	2.65	3.14	2.67	2.44
EXMEP	2.42	3.05	3.21	2.55	3.15	3.33	2.71	3.32	3.26
IMEPg	4.58	4.67	4.96	4.97	4.94	5.20	5.00	4.85	4.90
PMEP	0.81	0.82	0.77	0.50	0.52	0.65	0.63	0.65	0.68
IMEPn	3.78	3.86	4.20	4.47	4.42	4.56	4.37	4.20	4.21
	Second set of experiments								
FuelMEP	22.27	23.04	22.45	22.16	21.65	22.04	22.51	20.85	22.63
HTMEP	5.45	5.18	4.68	5.34	4.59	4.81	5.28	4.00	4.73
EXMEP	5.87	6.96	6.65	5.84	6.54	6.55	6.27	6.72	7.10
IMEPg	10.92	10.88	11.08	10.94	10.49	10.65	10.95	10.09	10.78
PMEP	1.17	1.39	1.12	1.07	1.08	1.28	1.37	1.33	1.57
IMEPn	9.75	9.49	9.96	9.88	9.41	9.37	9.58	8.76	9.21

[1] "MIN EGR" for the first and second sets of experiments denotes 17%- and 10%-EGR, respectively.
[2] "MAX EGR" for the first and second sets of experiments denotes 39%- and 52%-EGR, respectively.

Appendix B

Lambda Matrix for the First Set of Experiments

	CDC	Isobaric	Isobaric
0%	3.0	3.0	4.1
17%	2.4	2.5	3.3
39%	1.9	1.9	2.8

Lambda Matrix for the Second Set of Experiments

	CDC	Isobaric	Isobaric
0%	3.3	3.3	4.4
10%	3.0	3.2	4.2
52%	1.8	1.8	2.2